Mission Research Corporation

MRC/WDC-R-230

Copy 2

# The DIMEX Experiment

John Brandenburg
W. Michael Bollen
Robert Seeley
Khanh Nguyen

Final Report

September 25, 1990

Prepared for: Air Force Office of Scientific Research
Bolling Air Force Base
Washington, DC 20332

Contract No. F49620-89-C-0106



Prepared by: MISSION RESEARCH CORPORATION
8560 Cinderbed Road, Suite 700
Newington, VA 22122
(703) 339-6500

Research sponsored by the Air Force Office of Scientific Research (AFSC), under Contract F49620-89-C-0106. The United States Government is authorized to reproduce and distribute reprints for governmental purposes notwithstanding any copyright notation hereon.

# REPORT DOCUMENTATION PAGE

Form Approved
OMB No. 0704-0188



| 1. AGENCY USE ONLY (Leave blank) | 2. REPORT DATE | 3. REPORT TYPE AND DATES COVERED |
|---|---|---|
| | | Final Report/01 Aug 89-31 Jul 90 |

**4. TITLE AND SUBTITLE**

The DIMEX Experiment

**5. FUNDING NUMBERS**

61102F/2301/A8

**6. AUTHOR(S)**

John Brandenburg, W. Michael Bollen,
Robert Seeley, and Khanh Nguyen

**7. PERFORMING ORGANIZATION NAME(S) AND ADDRESS(ES)**

Mission Research Corporation
8560 Cinderbed Road, Suite 700
Newington, VA 22122

**8. PERFORMING ORGANIZATION REPORT NUMBER**

AFOSR-TR- 90 1075

**9. SPONSORING/MONITORING AGENCY NAME(S) AND ADDRESS(ES)**

AFOSR/NP
Bolling AFB DC 20332-6448

**10. SPONSORING/MONITORING AGENCY REPORT NUMBER**

F49620-89-C-0106

**11. SUPPLEMENTARY NOTES**

**12a. DISTRIBUTION AVAILABILITY STATEMENT**

Approved for public release; distribution is unlimited.

**12b. DISTRIBUTION CODE**

**13. ABSTRACT** (Maximum 200 words)

DIMEX (DIpole plasma Microwave EXposure) experiment has demonstrated both stable confinement of plasma at electron densities of the order of $10^{11}$ $cm^{-3}$ and electron temperatures of 1 eV and also has demonstrated strong absorption of 1 GHz microwaves with much reduced reflection (-10dB). In addition, high-intensity microwaves (greater than 0.1 $W/cm^2$) were strongly reflected, indicating that the plasma shell can function as a cloak to radar and a shield to HPM. It is believed that the successful demonstration of plasma confinement, cloaking to low-intensity microwaves, and even shielding to high-intensity microwaves can be explained in terms of exiting theory, drawn from the magnetic and laser fusion communities.

**14. SUBJECT TERMS**

Dipole, plasma, microwave, exposure

**15. NUMBER OF PAGES**

66

**16. PRICE CODE**

UL

| 17. SECURITY CLASSIFICATION OF REPORT | 18. SECURITY CLASSIFICATION OF THIS PAGE | 19. SECURITY CLASSIFICATION OF ABSTRACT | 20. LIMITATION OF ABSTRACT |
|---|---|---|---|
| UNCLASSIFIED | UNCLASSIFIED | UNCLASSIFIED | SAR |

## TABLE OF CONTENTS

## TABLE OF CONTENTS (Concluded)

## LIST OF ILLUSTRATIONS

## LIST OF ILLUSTRATIONS (Concluded)

# SECTION 1

# INTRODUCTION: THE DIMEX EXPERIMENT

## 1.1 MOTIVATION AND GOALS OF THE DIMEX EXPERIMENT.

The goal of the DIMEX (DIpole plasma Microwave EXposure) experiment is to explore the feasibility of using a low temperature, magnetically confined plasma as a "plasma cloak" to hide the satellite from radar. The possibility that the plasma might act as a shield to high-intensity EM (ElectroMagnetic) threats such as nuclear EMP (EM Pulse) and HPM (High-Power Microwaves) is also explored. The DIMEX experiment was proposed because of theoretical arguments that such a concept was feasible. To further verify the feasibility of this concept, DIMEX was to demonstrate two effects:

(1) Magnetic confinement of a plasma with a density on the order of $10^{11}$ $cm^{-3}$ and temperature of $\sim$ 1 eV (11,000 K) in a shell around a dipole magnet with a field of a few 100 gauss.

(2) Strong absorption of GHz range microwaves by the plasma at low EM field intensities.

DIMEX has demonstrated both stable confinement of plasma at electron densities of the order of $10^{11}$ $cm^{-3}$ and electron temperatures of 1 eV and also has demonstrated strong absorption of 1 GHz microwaves with much reduced reflection (-10 dB). In addition, high-intensity microwaves (>0.1 $W/cm^2$) were strongly reflected, indicating that the plasma shell can function as a cloak to radar and a shield to HPM. We believe that the successful demonstration of plasma confinement, cloaking to low-intensity microwaves, and even shielding to high-intensity microwaves can be explained in terms of existing theory, drawn from the magnetic and laser fusion communities.

## 1.2 OBSERVATIONS ON THE THEORY OF DIMEX PLASMAS AND INTERACTIONS.

The DIMEX experiment was proposed because of the theoretical understanding that by using the technique of "line tying"[1], a region of plasma could be stably confined around a dipole magnet in a "shell" configuration: low plasma density near the magnet rising to maximum density some distance away and then monotonically decreasing in density out to infinity. Confinement of plasmas in dipole magnetic fields is well understood theoretically and is observed in planetary magnetospheres [2] and magnetic confinement fusion experiments.

Absorption of microwaves by collisional, and linear and nonlinear wave conversion processes (i.e. processes which convert EM waves to plasma waves) are well understood from laser fusion studies and experiments, at least as far as basic mechanisms are concerned. However, exact values of absorption coefficients for EM waves may depend on detailed nonlinear calculations involving plasma profiles and other factors. Generally propagation of an electromagnetic wave in a plasma involves induced motion of electrons by the E(electric) field of the EM wave. This motion can produce a *linear density oscillation in the electrons* if the motion has components parallel to a plasma density gradient, through either direct motion induced by the EM wave or indirect motion induced by the action of a B field in the plasma on the EM electron motion. In either case EM wave energy does work on the electron density distribution, and EM energy is transformed into plasma wave energy. This effect can occur even at low EM wave intensities and is termed linear conversion. In addition, nonlinear processes can occur at high EM wave intensities and convert EM waves into plasma waves, leading to absorption of EM energy.

Based on theories refined and developed in the magnetic and laser fusion efforts and astrophysical explorations, it was believed that the DIMEX experiment had a good chance of success, and that its phenomena could be explained theoretically. This has proved to be the case. Accordingly, the DIMEX effort is not only a success as an experiment, but it is also a success in terms of application of plasma theory borrowed from the magnetic fusion and laser fusion communities.

## 1.3 REPORT OVERVIEW.

In the remainder of this report the Dimex apparatus and experimental results will be discussed. Also, we will present a theoretical analysis of the DIMEX experimental results. Finally, a section will summarize the DIMEX project conclusions.

# SECTION 2

# EXPERIMENTAL RESULTS

## 2.1 INTRODUCTION.

### 2.1.1 Purpose of the Experiment.

The purpose of the DIMEX experiment was twofold: first to demonstrate that reasonable confinement time of a plasma with the properties necessary for a cloaking plasma ($n_i \sim 10^{11}$ cm$^{-3}$, $T_e \sim 1$ eV, and $T_e/T_i \sim 40$) is possible and, second, to begin an investigation of how such a plasma will interact with microwave radiation. As shown later in this section, both purposes were accomplished. Confinement of $10^{11}$ cm$^{-3}$ plasmas was observed and strong absorption of microwave radiation was demonstrated.

### 2.1.2 Summary of the Experimental Results.

The DIMEX experiment was designed to be a pulsed experiment to allow the confinement time of the plasma to be measured. The experiment showed that for the experimental geometry and the plasma production method used, stable confinement exists for about 1 ms, after which instabilities occur which cause the plasma to decay with an e-folding time of $\sim$ 0.5 - 1 ms. It should be possible to greatly enhance the plasma confinement time. We believe that two effects are presently contributing to the instabilities that result in plasma loss. The first is the fact that the experimental chamber is small compared to the magnetically confined volume. Thus, many magnetic field lines terminate on the chamber walls resulting in loss of confined plasma to the walls. Secondly, the plasma is created by applying a burst of modest-energy ionization electrons and studying the plasma in the after glow. The initial plasma density profile established by this method is far from uniform. Rapid decay to the observed "stable" profile occurs. However, we now believe that the seeds of instability are planted in this non-equilibrium approach to generating the plasma. A better approach will be

to create a dc plasma using electrons created along the confining magnetic field lines. Future work should focus on how to create a more stable, low-loss, confined plasma.

In addition to the plasma confinement experiment, we investigated the interaction between microwaves and the confined plasma. As expected there is a strong interaction. The experiment was designed to measure relative absorption and is just the first step in investigating the interaction. Results were encouraging. Relative power absorption on the order of -10 dB was observed, i.e. the signal reflected from the magnet assembly with plasma was 10 times less than with no plasma. We also observed that under certain conditions the microwaves were refracted around the magnet assembly when the plasma was present. Finally, we observed that the reflection and transmission properties vary depending on the polarization of the incident microwaves. This is understandable since in one orientation the electric field is essentially along the magnetic field. For this case the plasma is one-dimensional and resonant absorption would be expected to dominate. For the other polarization, the electric field is perpendicular to the background magnetic field and cyclotron absorption (i.e., magnetic effects) become important. The details are described later.

## 2.2 DESCRIPTION OF THE EXPERIMENT

### 2.2.1 Experimental Chamber.

The DIMEX plasma chamber is a 45-cm diameter cylindrical vacuum chamber which is 43 cm long. L-band microwave waveguide penetrates from two sides, allowing microwaves to be transmitted through the chamber. The permanent magnet assembly used to confine the plasma is supported from above and a $LaB_6$ cathode assembly is used to create the ionizing electron beam. A schematic of the DIMEX plasma chamber is shown in Figure 2.1. Also shown are the typical locations of the Langmuir probes used for measuring the plasma density. Figure 2.2 is a photograph of the DIMEX experiment showing the plasma chamber and the associated power supplies, support equipment, and recording instrumentation.

The primary diagnostic for the experiment was a Langmuir probe to measure the ion density. The plasma is approximately neutral so the ion density, electron density, and plasma density are all the same value. The Langmuir probe is used

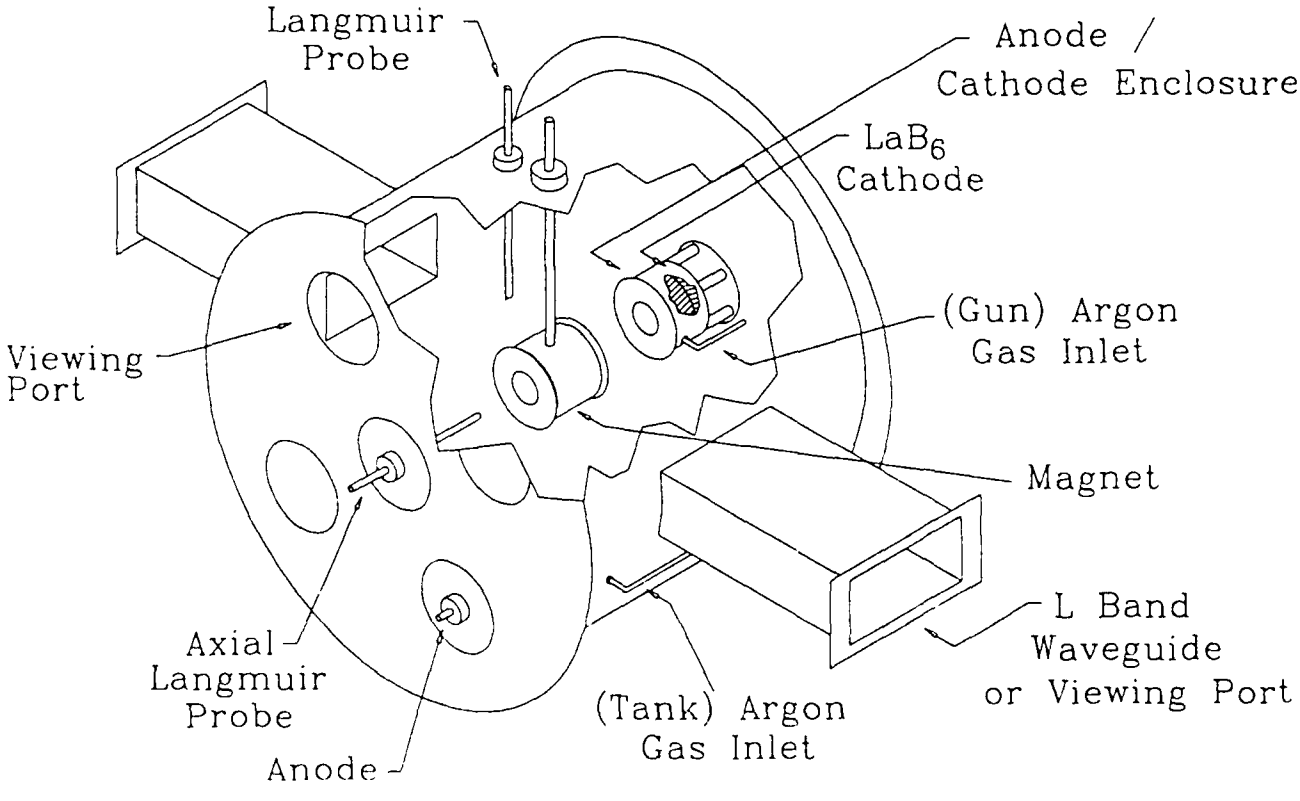


**Figure 2.1. Schematic drawing of the DIMEX plasma chamber.**

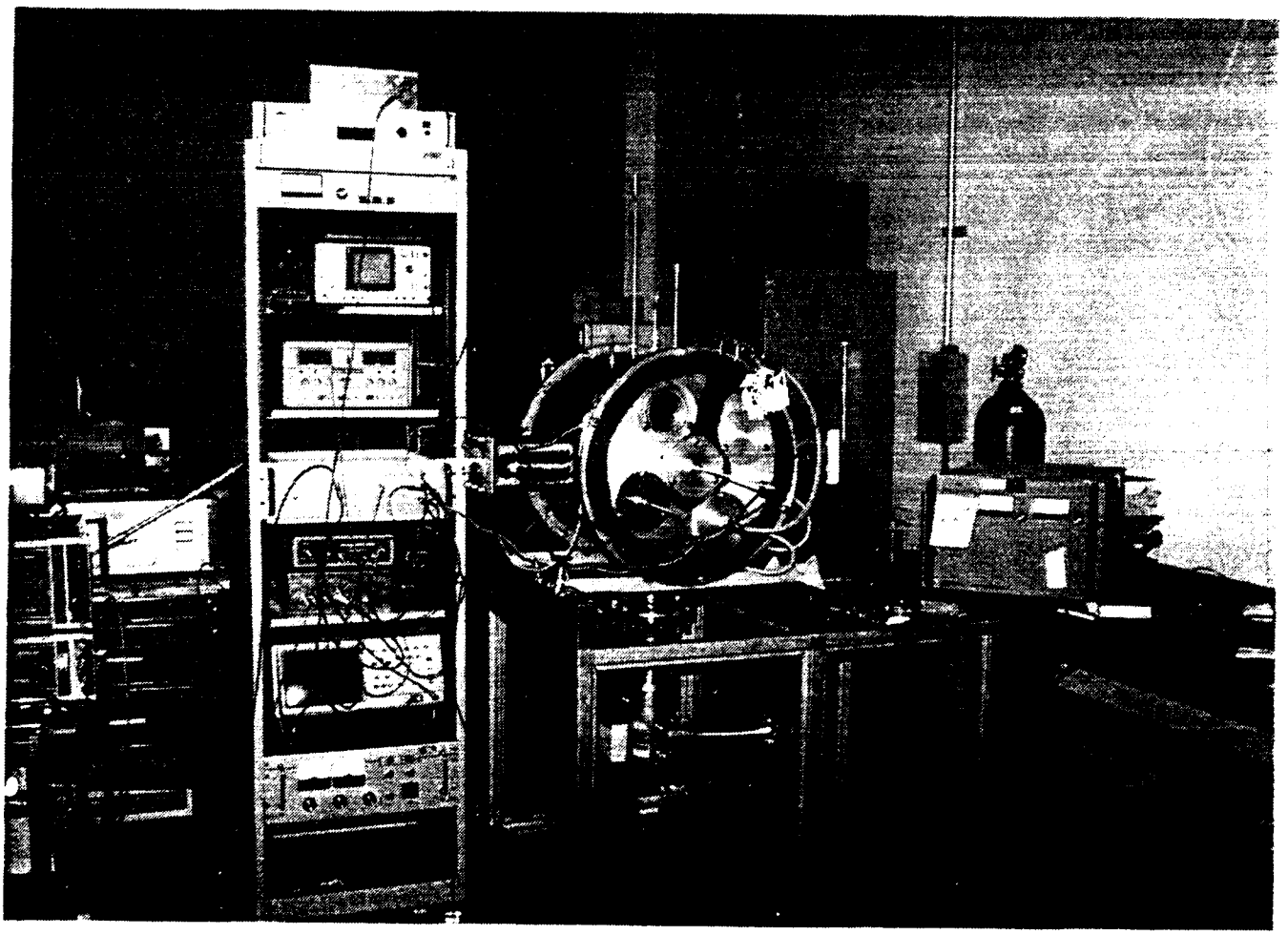

Figure 2.2. Photograph of the DIMEX experimental apparatus.

to measure the ion saturation current. The ion density is then calculated using the following equation:

$$I_i = 0.46 e A_p n_i \sqrt{\frac{|e\theta|}{m_i}} \tag{2.1}$$

where the theory of Lafromboise [3] has been employed, and the variables are defined below:

$A_p$ = probe surface area,
$\theta$ = probe potential compared to the plasma potential,
$n_i$ = ion density,
$I_i$ = ion saturation current collected by the probe, and
$m_i$ = ion mass.

This equation is valid for the ratio of the cylindrical probe radius to the Debye length less than 3 and for the ratio of $e\theta/(kT_e) > 1$ where $kT_e$ is the electron energy. This equation does not include magnetic field effects. In general our measurements were made where the ion and electron gyro radius were larger than the Debye length and the probe diameter and, therefore, Equation (2.1) is valid. For low density ($n_i < 10^9$) or high magnetic field (B > 1000 gauss), Equation (2.1) will begin to become incorrect [4]. The electron and ion temperatures were not measured. However, this type of plasma typically has ion temperatures of about .025 eV and electron temperatures of about 1 eV. However, sometime during the afterglow, the electron temperature will begin to drop rapidly since the "hot" electrons are lost first to the chamber walls.

### 2.2.2 Magnetic Field Generation.

The approach to radar cloaking that DIMEX investigates is that of a plasma absorber surrounding an asset. The plasma is held in place by a dc magnetic field in a manner similar to that used in magnetic confinement fusion (except the ion temperatures are much lower, allowing long confinement times). For the DIMEX experiment, the dc magnetic field is supplied by a permanent magnet assembly. A photograph of one such assembly is shown in Figure 2.3. We used two different

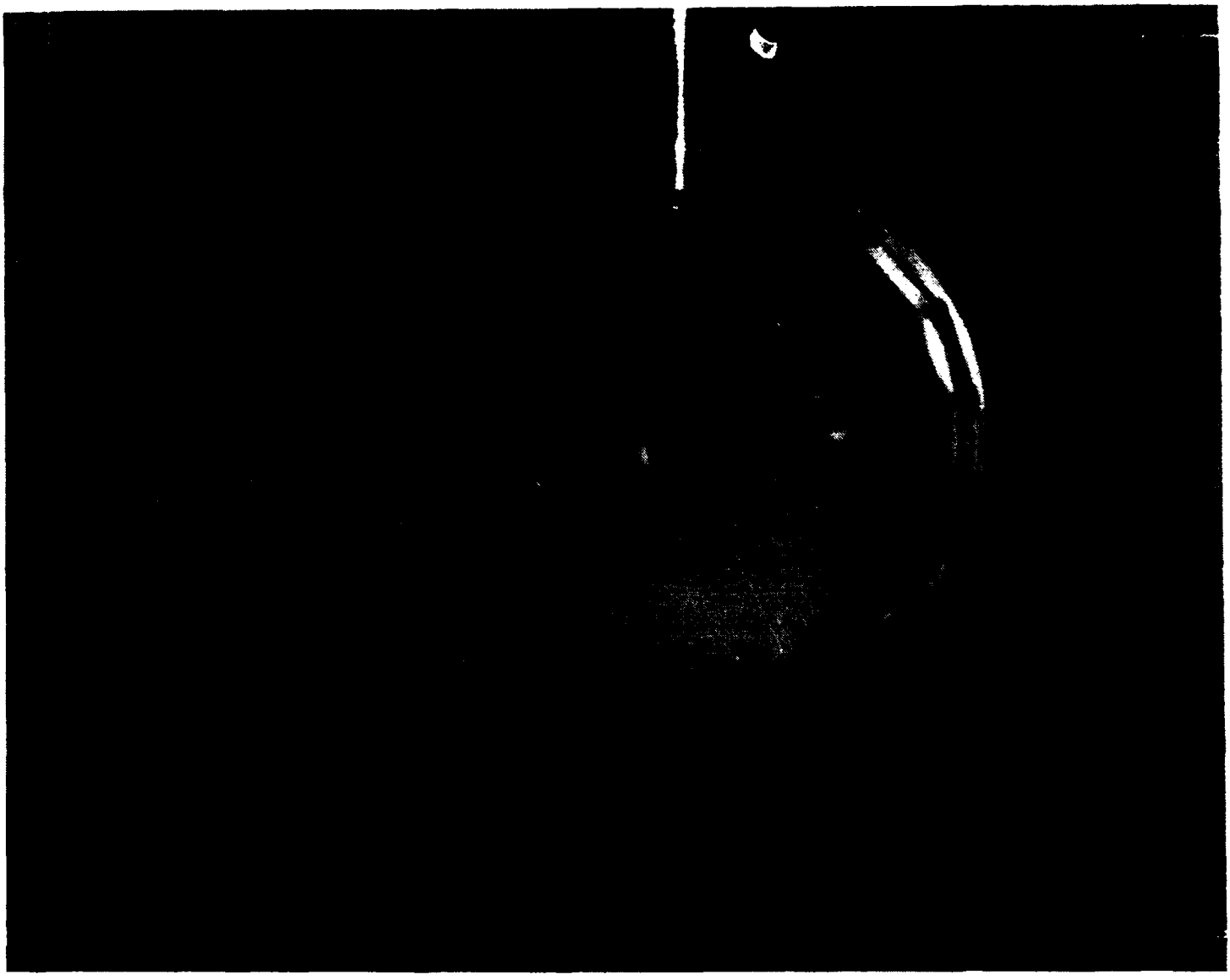

Figure 2.3. Photograph of the DIMEX large magnet assembly.

diameter magnet assemblies which are shown schematically in Figures 2.4 and 2.5.

We performed the initial studies with the large diameter magnet assembly and quickly moved to the small magnet assembly, with which we performed most of the experiments, when it became clear that the intersection of the magnetic field lines with the chamber walls was affecting the confinement time. The permanent magnets were rings with the characteristics shown in Figure 2.6. Multiple magnet rings were stacked to form a solenoidal magnet structure with an aspect ratio of 1. The entire assembly was sheathed in a stainless steel shell. In addition, a disk was placed just in front of the end facing the electron gun to provide a heat shield. This heat shield also provided line tying of the magnetic field lines. The center hole was aligned to allow any high-energy electrons from the gun to pass directly through the assembly.

The axial magnetic profiles for both the large and small magnet assemblies were measured and are shown in Figure 2.7. The location of the heat shield on the electron gun (cathode shield) and the end flange of the vacuum chamber are shown for reference. It should be noted that small nonuniformities in the magnetic field were measured. This is attributed to nonuniformities in the manufacture of the permanent magnet rings and may have contributed to the instabilities responsible for plasma loss. Future work will make use of a pulsed electromagnet designed to provide a uniform magnetic field for times long compared to the confinement time.

### 2.2.3 Electron Beam Source.

The plasma chamber is operated with a background argon gas pressure of $\sim 10^{-3}$ torr. The cloaking plasma is created by firing a burst of primary electrons ($kT_e \sim 300$ eV) into the dc magnetic field. The primary electrons are generated using the $LaB_6$ electron gun shown in Figure 2.8. Figure 2.9 is a schematic of the gun assembly, and Figure 2.10 shows the electric circuit and biasing scheme used to generate the primary electron beam and the resulting background plasma. We tried two different biasing schemes. The best method was to keep the anode near ground, since this kept the plasma potential near ground and prevented arcing to the Langmuir probe.

The primary electron beam ionizes the argon gas, creating a plasma. The majority of the primary electrons are stopped and reflected as they approach the

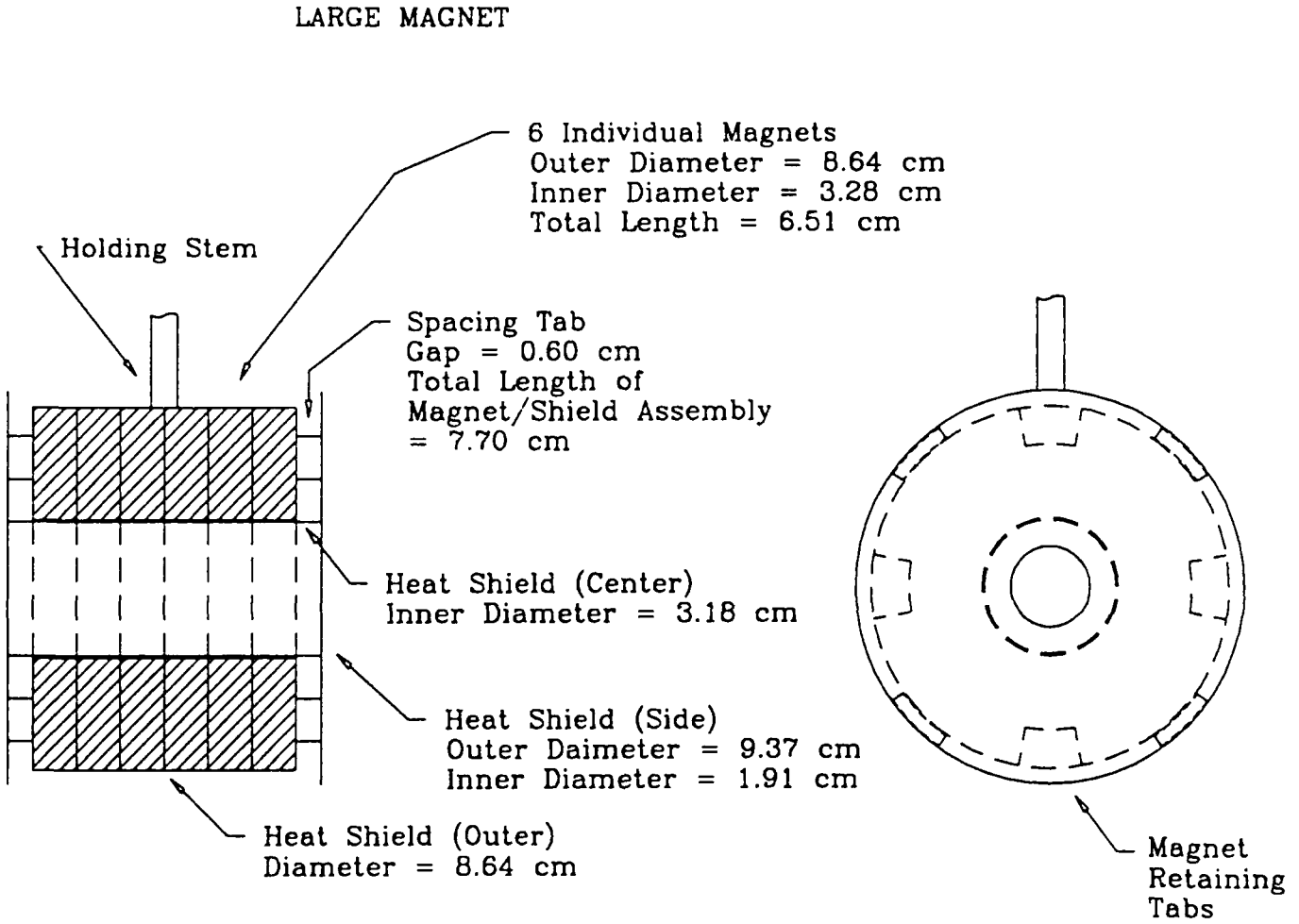


Figure 2.4. Schematic of large magnet assembly.

SMALL MAGNENT

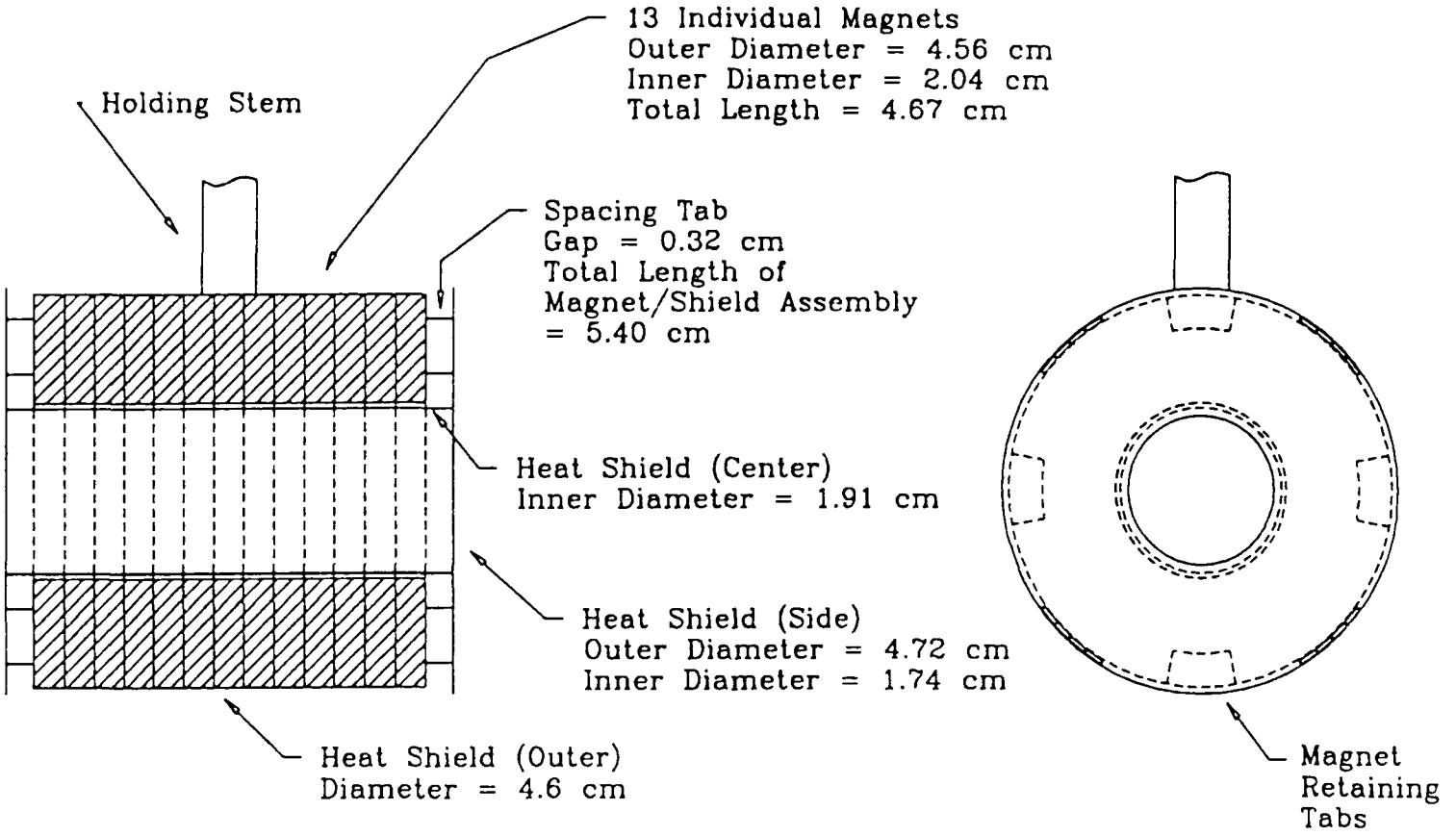


Figure 2.5. Schematic of small magnet assembly.

| | Outer Diameter | Inner Diameter | Thickness | Material |
|---|---|---|---|---|
| Small Magnet | 1.797 in. | .801 in. | 1.838 in. | Ceramic – Ferrite based combination of iron and other chemicals |
| Large Magnet | 3.398 in. | 1.288 in. | 2.550 in. | Same as small magnet composition |

Note: Source for material composition description was Edmund Scientific catalog.

**Figure 2.6. Table of magnet specifications.**

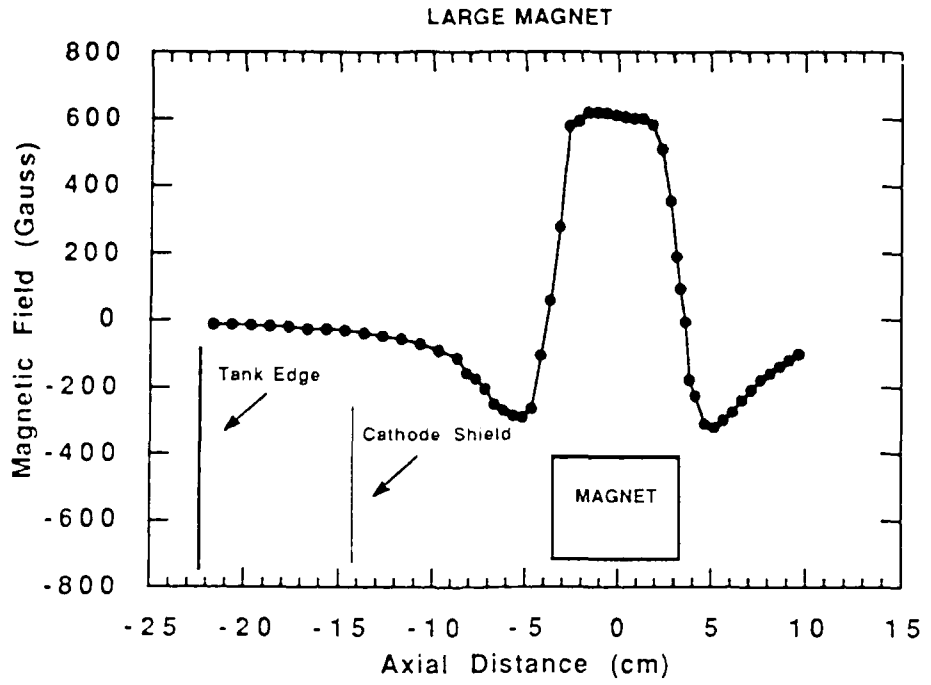


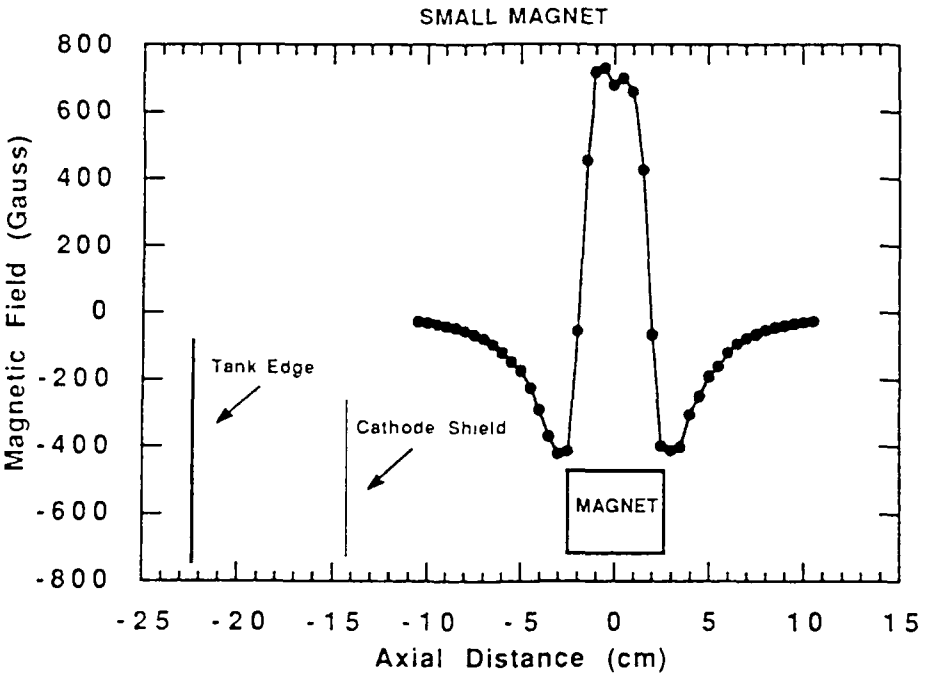


Figure 2.7. Magnetic field profiles for both the large and small magnet assemblies.

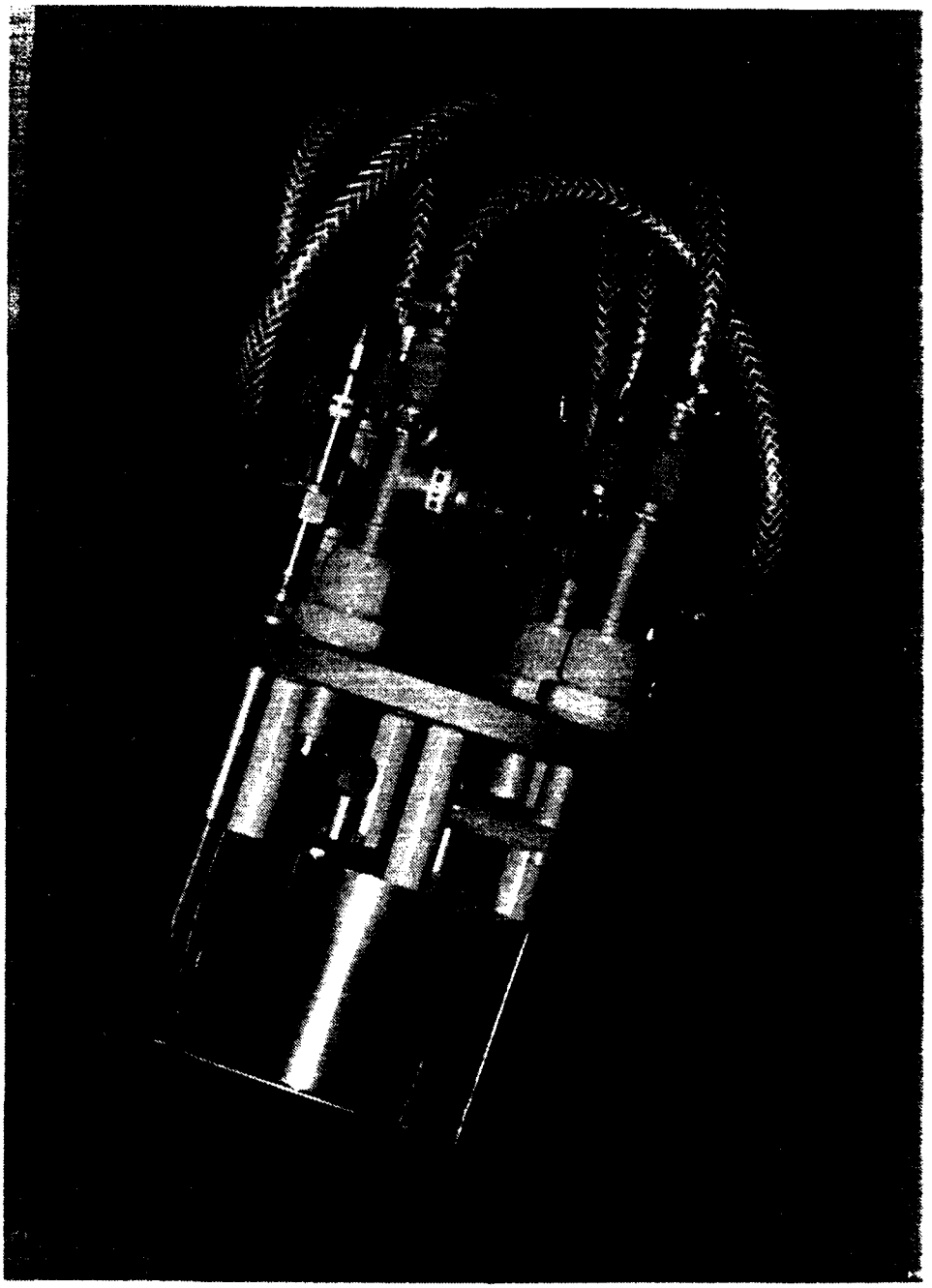

Figure 2.8. Photograph of the $LaB_6$ source assembly.

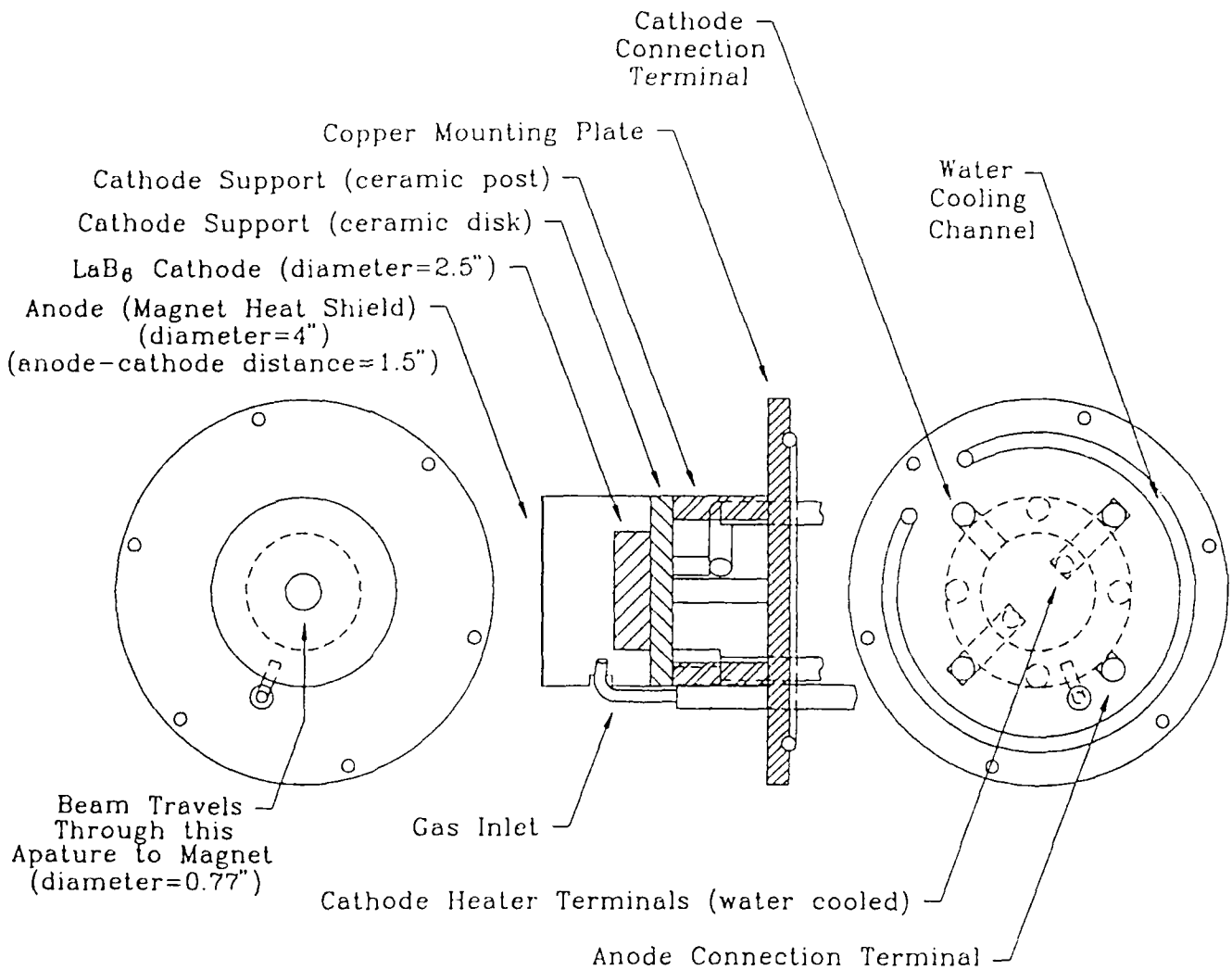


**Figure 2.9. Schematic of the $LaB_6$ source assembly.**

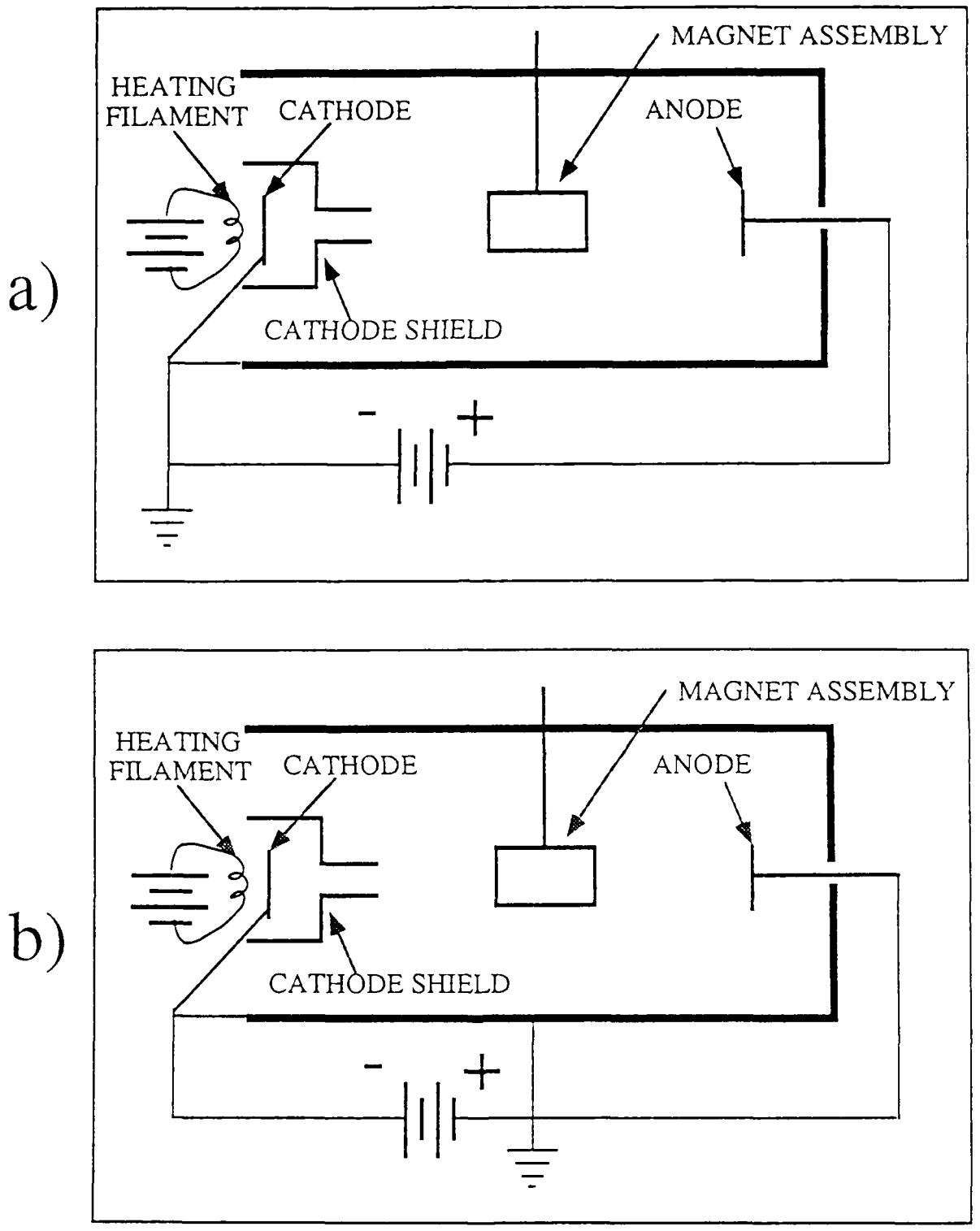


**Figure 2.10.** **Schematic for biasing $LaB_6$ cathode. a) anode at +270 V, and b) anode at ground.**

magnet assembly due to magnetic reflection. However, in the region where they are turned around, they cause a large amount of ionization. The plasma which is created is "born" on field lines and is therefore trapped. It quickly diffuses along the field lines after the primary electron beam is pulsed off to form a trapped plasma .

Figure 2.11 shows the measurement of the plasma density created by the primary electron beam with no magnet assembly present. Figure 2.12 shows the same plasma density profiles, but with the magnet assembly present. The magnet has some effect in confining the plasma. However, other effects which we do not presently understand are also responsible for confinement. Figure 2.13 shows the effect on the floating potential of using the two different anode biasing schemes. There is only limited data for the case of biasing the anode at +270 volts because of arcing to the probe.

## 2.3 MAGNETIC CONFINEMENT OF THE PLASMA

### 2.3.1 Confined Plasma Structure.

Recall that the first objective of the DIMEX experiment was to demonstrate confinement of a plasma using a dipole magnetic field. Figure 2.14 is a plot of a number of time histories of the plasma density at different radial positions from the magnet assembly. The first spike in the density is due to the plasma formation while the primary electron beam is on. When the beam is turned off, the density rapidly decays and then stabilizes, giving a constant density for about 1 ms after which the plasma slowly decays. Figure 2.15 contrasts the confinement time with a magnetic field to one without a magnetic field, clearly demonstrating that we have achieved magnetic confinement at the desired $10^{11}$ cm$^{-3}$ plasma density. Although the magnetic field appears responsible for the plateau at 1 ms, we do not presently understand the long delay time seen for no magnetic field.

Figure 2.12 shows radial and axial scans of the plasma density as measured just after the primary electron beam is turned off ($\tau = 0$ $\mu$s) and for the $\sim$ 1 ms constant density plateau ($\tau = 860$ $\mu$s) using the small magnet assembly. (The convention of referring to time *after* the electron beam is turned of is used since different pulse length primary electron beams were used. However, all density/time plots show a time

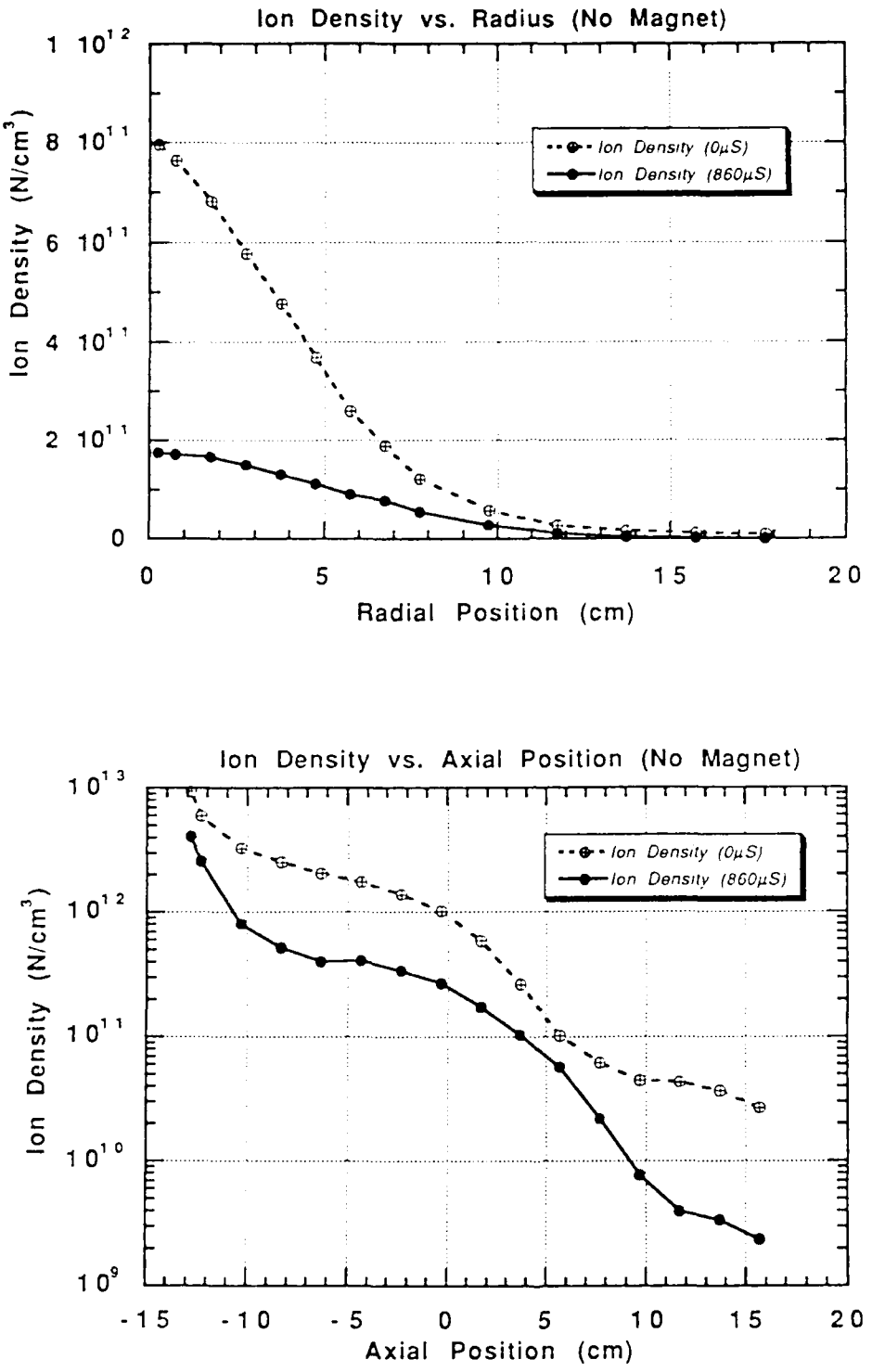


**Figure 2.11.** Plot of ion density radial and axial profiles with no confinement magnet.

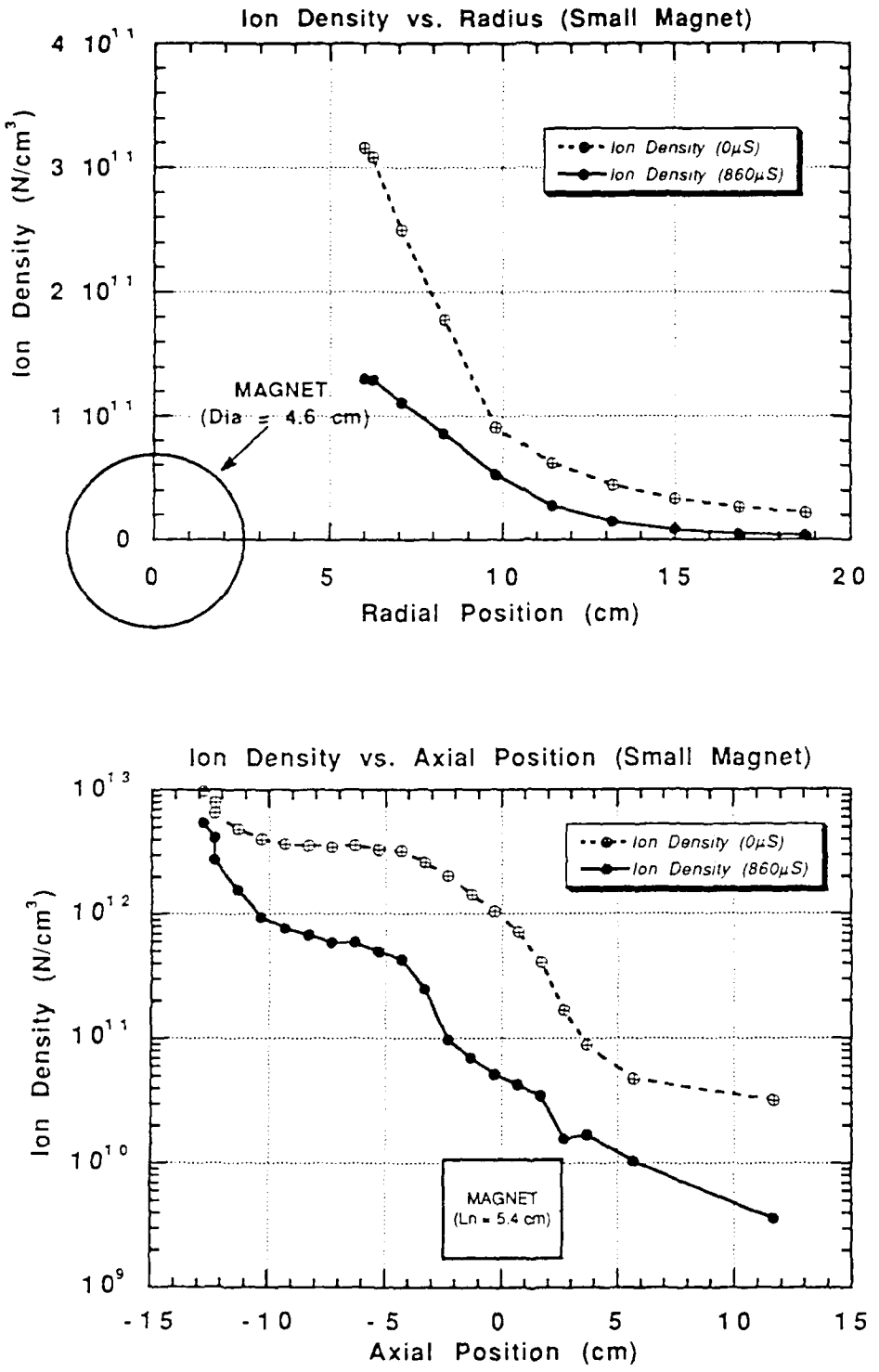


**Figure 2.12.** Radial and axial profiles of the plasma density with the small magnetic assembly.

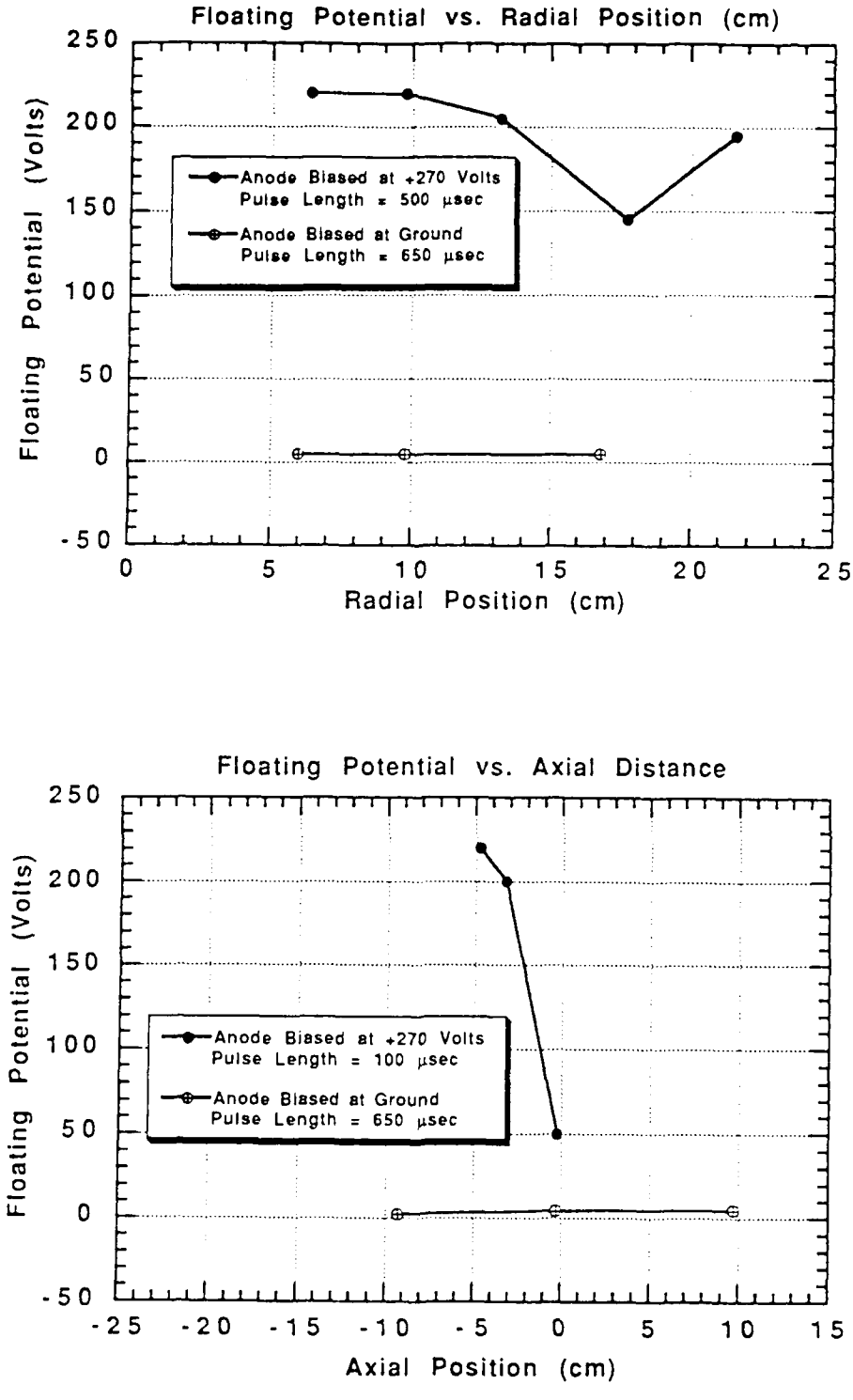


Figure 2.13. Floating potential for different biasing schemes.

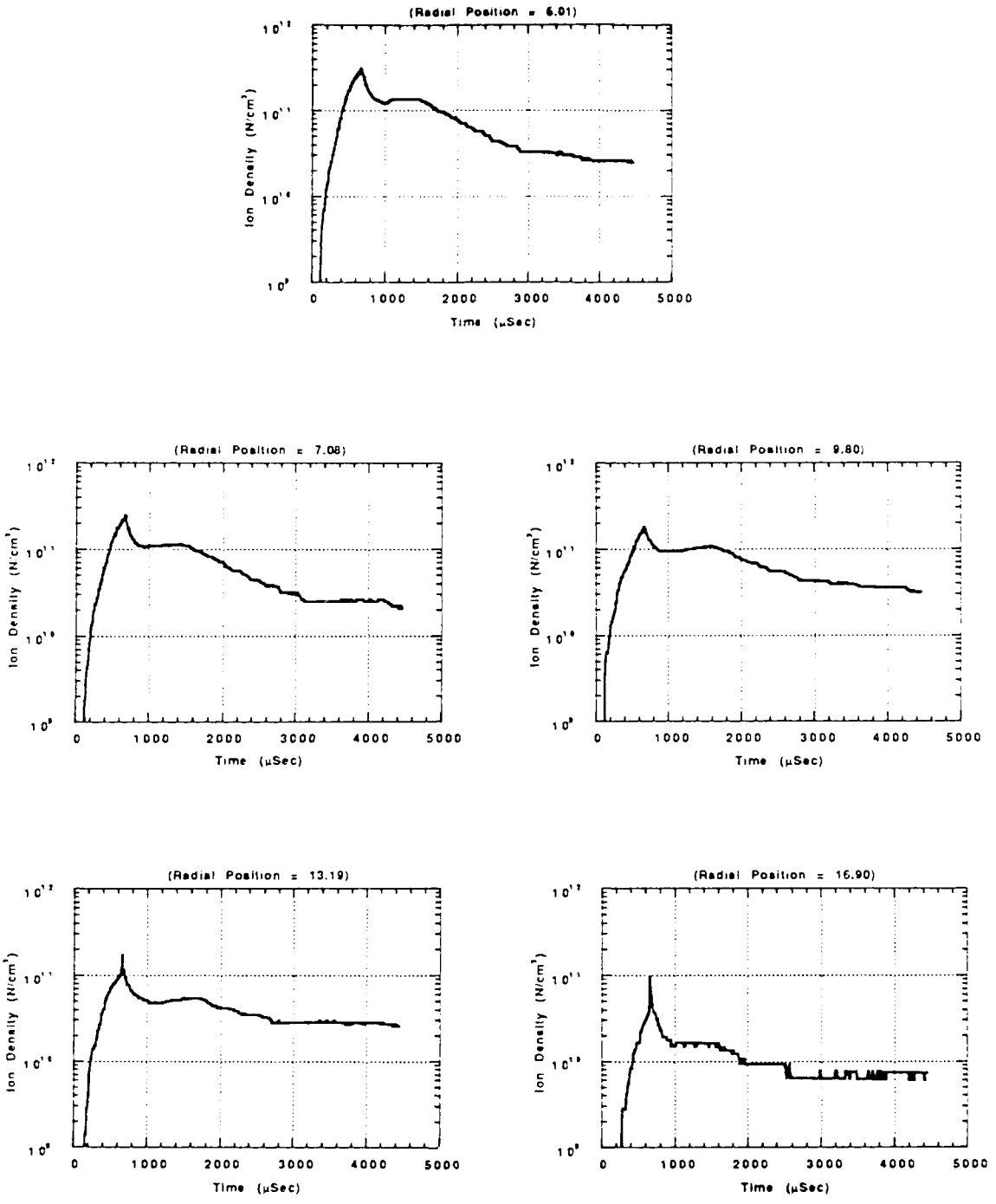


Figure 2.14. Time histories of the radial plasma density profile for the magnetic confinement plasma (6 scope traces).

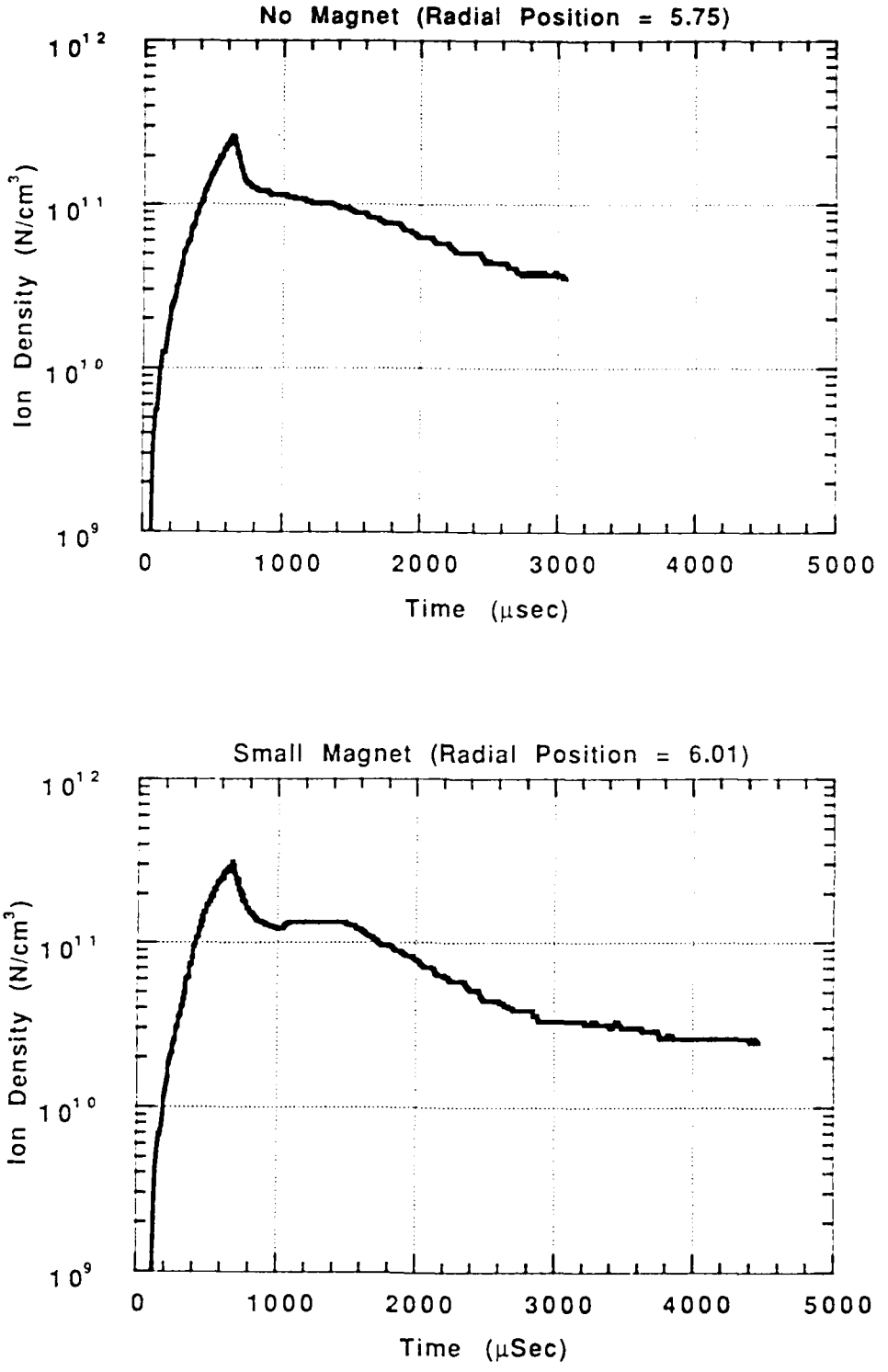


Figure 2.15. Comparison of plasma confinement time with and without a magnetic field.

axis with $t = 0$ being the start of the pulse.) Some reasons for the stabilization to be disrupted become immediately apparent. As expected there are density gradients in the radial direction, but these decrease from 0 to 860 $\mu$s. Unexpectedly, however, there are very large density gradients in the axial direction at 860 $\mu$s. Initially, due to the fact that the primary electron beam is reflected on one side (negative axial position), we expect a density gradient. However, we expected that during the initial decay the plasma would flow along field lines, developing a uniform density and establishing the stable density plateau in time. This is apparently not the case.

Figure 2.16 shows another important fact about the plasma geometry. This figure shows a radial plasma density scan for the large magnet assembly. Our Langmuir probe is in a fixed location and actually measures along a chord; we then convert the chord position to the equivalent radial position. Therefore, for the larger magnet assembly we are able to measure closer to the magnet (i.e., $r/r_0$ is smaller, where $r$ is the radial distance from the axis and $r_0$ is the magnet assembly radius). What Figure 2.16 clearly shows is a "shell" structure to the plasma. This means that near the magnet there is very little plasma. This is extremely important for satellite cloaking where it would be desirable to keep the satellite exterior away from the cloaking plasma.

Figure 2.16 also compares radial plasma density scans for the two magnet assemblies under similar conditions. Recall that the aspect ratio of the magnetic field is kept the same for both cases. The larger density for the small magnet assembly is as expected, based upon the fact that fewer magnetic field lines intersect the DIMEX chamber walls.

We have observed stable plasma confinement times $\sim$ 1 ms, and Figure 2.15 shows that this is an improvement over the plasma lifetime without a magnetic field.

### 2.3.2 Effect of Pressure (Collisional Effects).

We also measured the effect of varying the background neutral argon pressure on the plasma density, and this is shown in Figure 2.17. As expected the density is approximately proportional to the pressure, since the ionization cross section increases with pressure. At about 0.1 torr the behavior changes. We believe that this is due to the fact that at this pressure the primary electron beam is being scattered

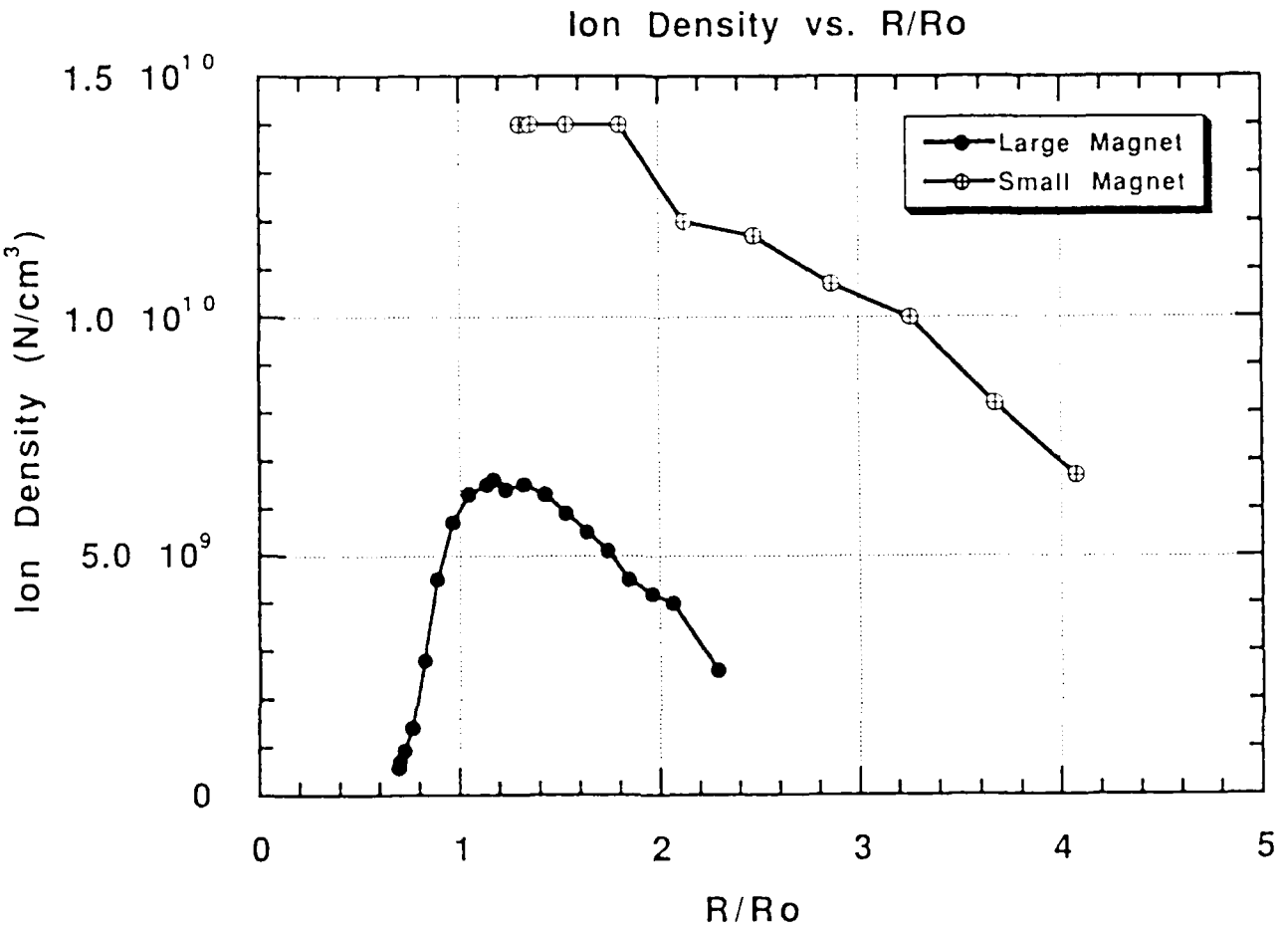


Figure 2.16. Radial profile of the plasma density with magnetic field. Note the "shell" structure in the large magnet data. Geometry constraints of the experimental set-up prevented the shell structure from being observed with the small magnet assembly (e.g., we could not get the Langmuir probe into the equivalent radial position).

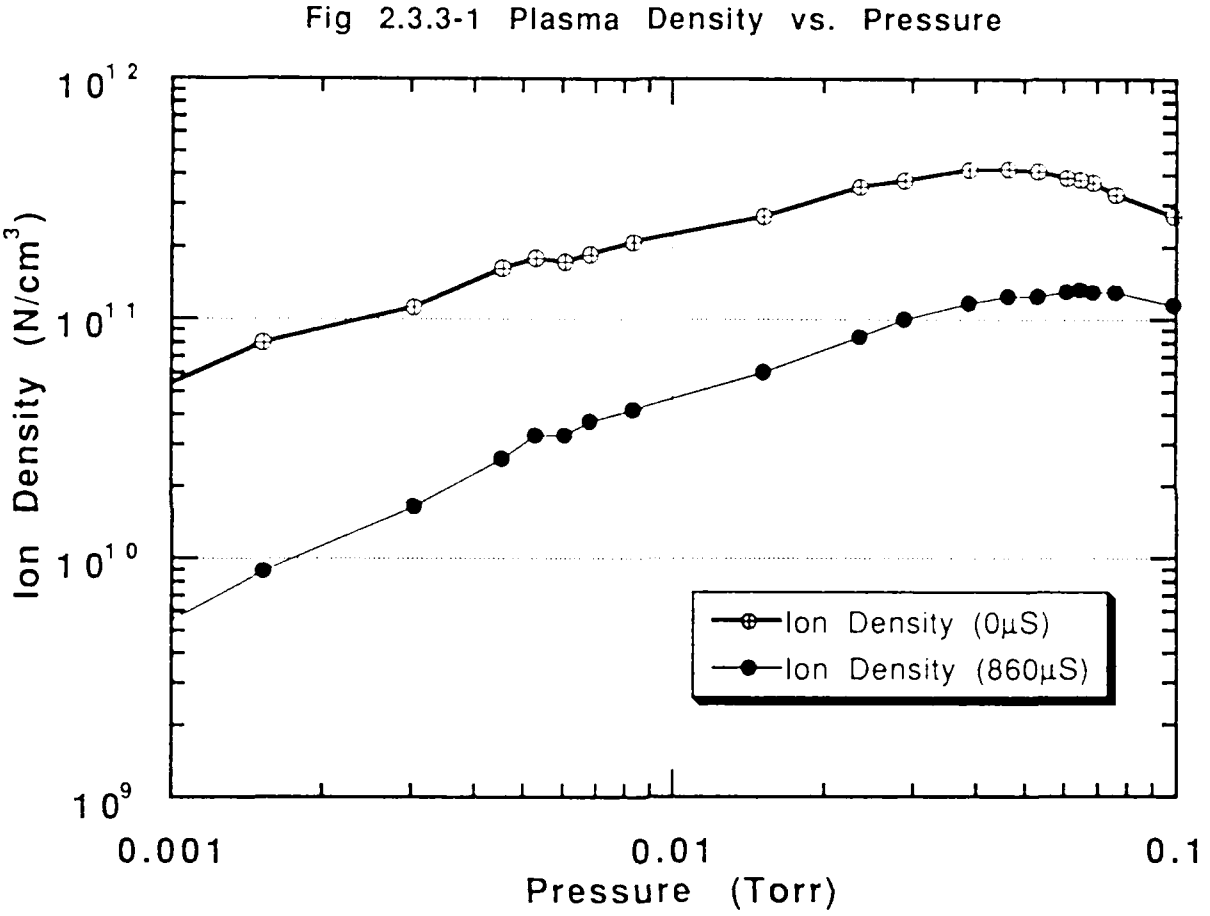


**Figure 2.17.** Plot of plasma density vs pressure.

prior to reaching the magnetic field. Another way to say this is that the mean free path has decreased to less than the separation distance between the magnet assembly and the cathode of the gun. Figure 2.18 is a plot that shows how the mean free path varies with pressure.

Figure 2.19 shows how the time history of the plasma density varies with background gas pressure. The first peak increases in density since as the pressure goes up the probability of an ionizing collision increases. We are not sure why the shape changes, but we assume it is because the loss mechanisms due to collisional diffusion and recombination increase and alter the time to reach equilibrium. Of most importance to us is that at a pressure of about 0.76 torr a stable density plateau forms. The start of such a plateau can be seen as early as 0.024 torr. In the follow-on work an understanding of the role of collisions in establishing the density plateau must be developed.

## 2.4 MICROWAVE INTERACTION WITH THE CONFINED PLASMA.

### 2.4.1 Introduction.

The next step in the experiment was to examine the interaction of microwaves with the magnetically confined plasma. A schematic of the microwave experiment is shown in Figure 2.20.

Experiments were performed at L-band (1-2 GHz) and S-band (2-4 GHz). The latter frequency was chosen because the waveguide was small enough to be inserted in the chamber L-band waveguides and rotated to allow both incident polarizations.

Figure 2.21 shows the two polarization cases examined in this work: 1) the electric field perpendicular to both the dc magnetic field, $B_0$, and the density gradient, $\nabla n$. and 2) the electric field parallel with $B_0$.

A third case exists which is the electric field parallel to the density gradient and perpendicular to $B_0$. We could not excite this case with the geometry in the present DIMEX experiment. It is excited by oblique incidence of the microwaves

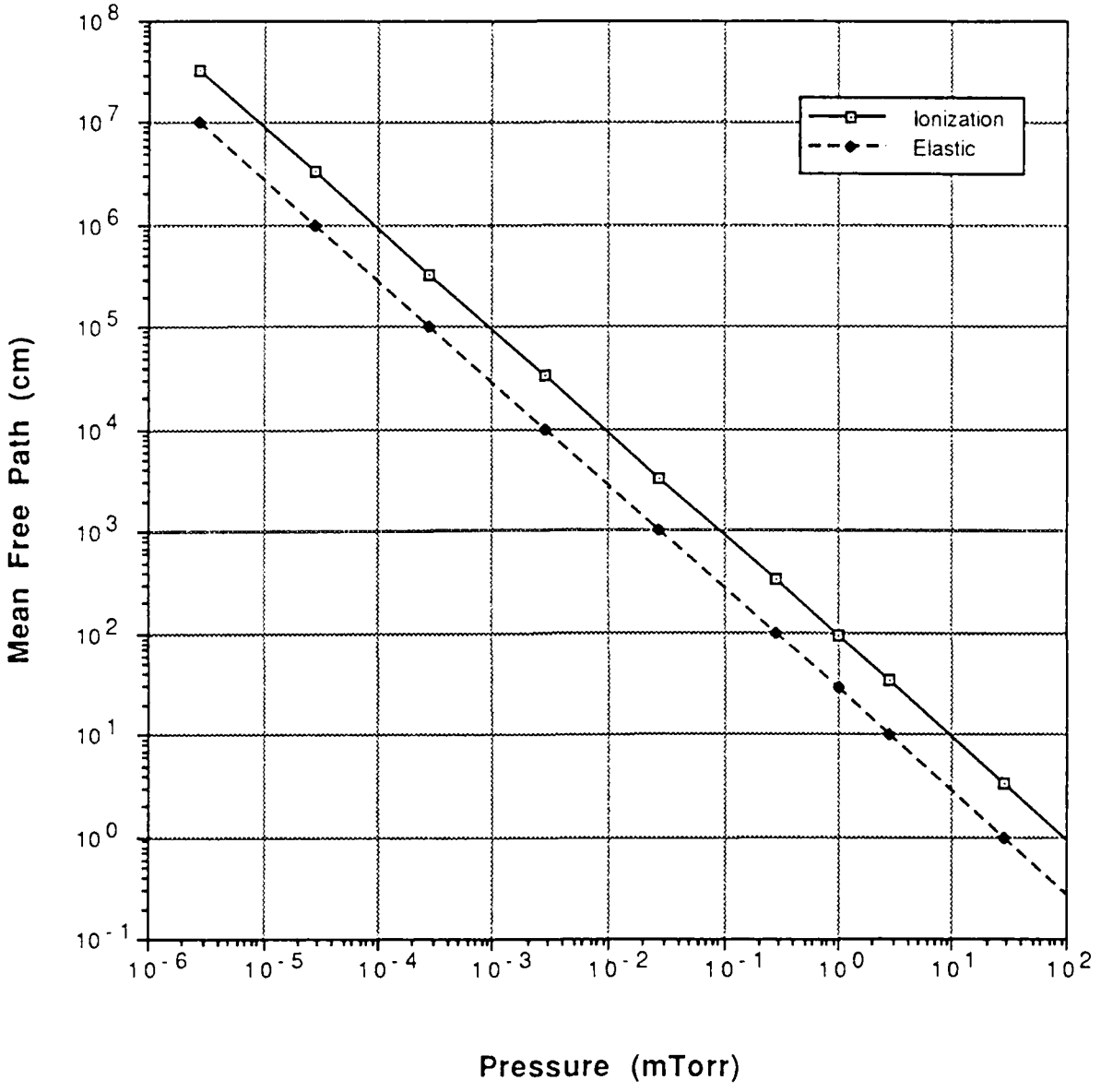


**Figure 2.18. Mean free path of primary electrons (300eV).**

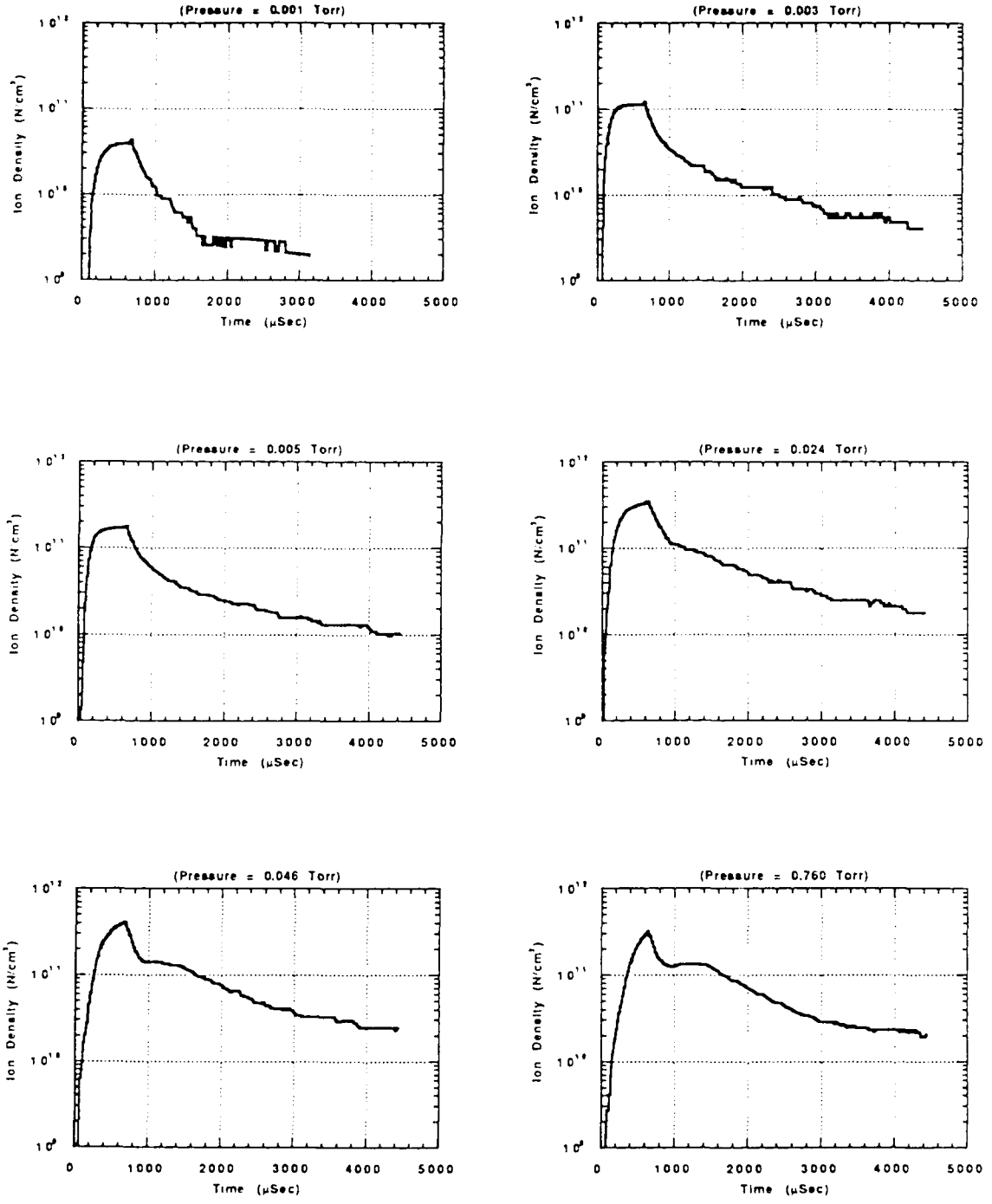


Figure 2.19. Time histories of the plasma density for various background pressures.

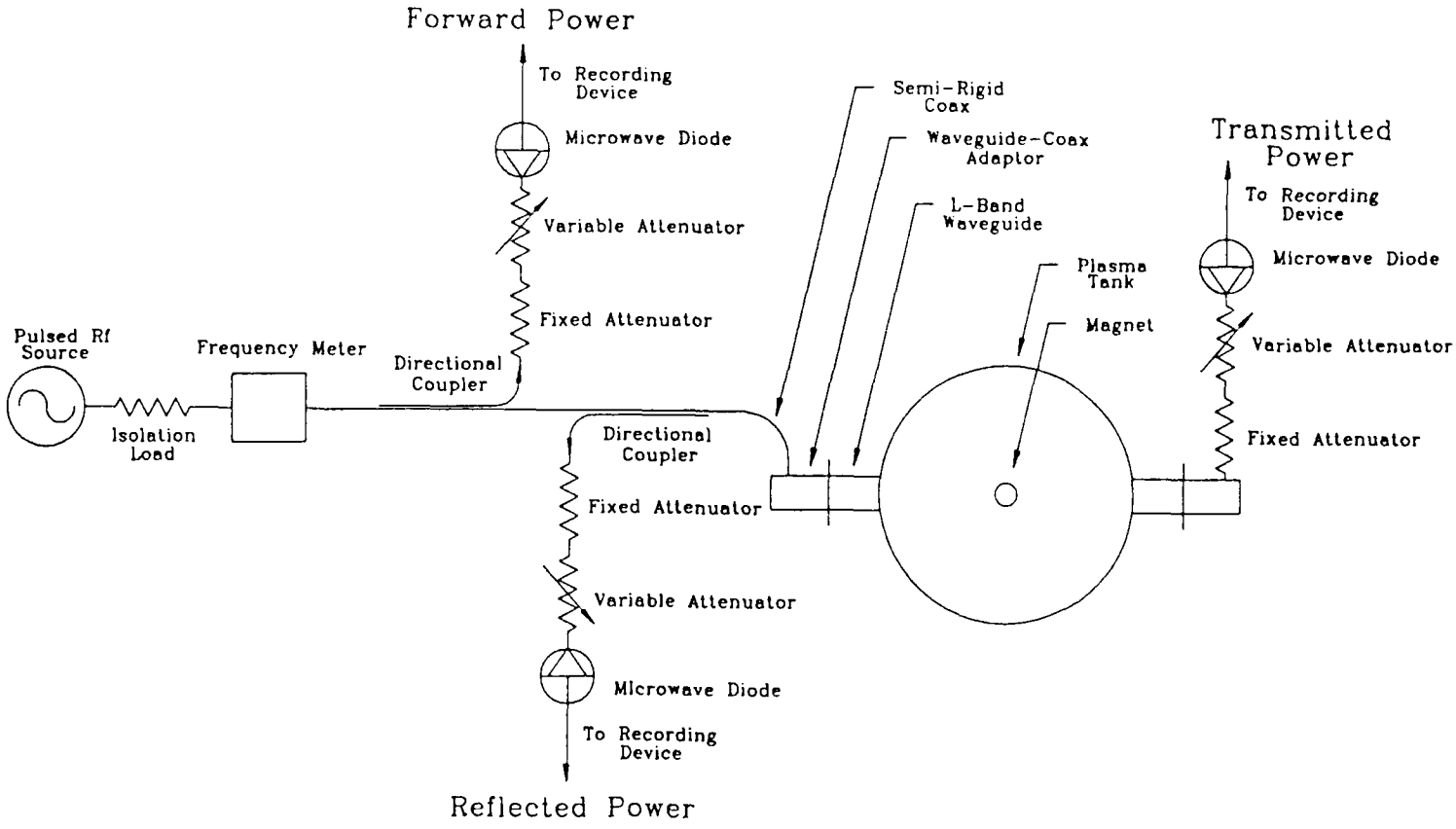


**Figure 2.20.** Schematic of the experimental microwave set-up.

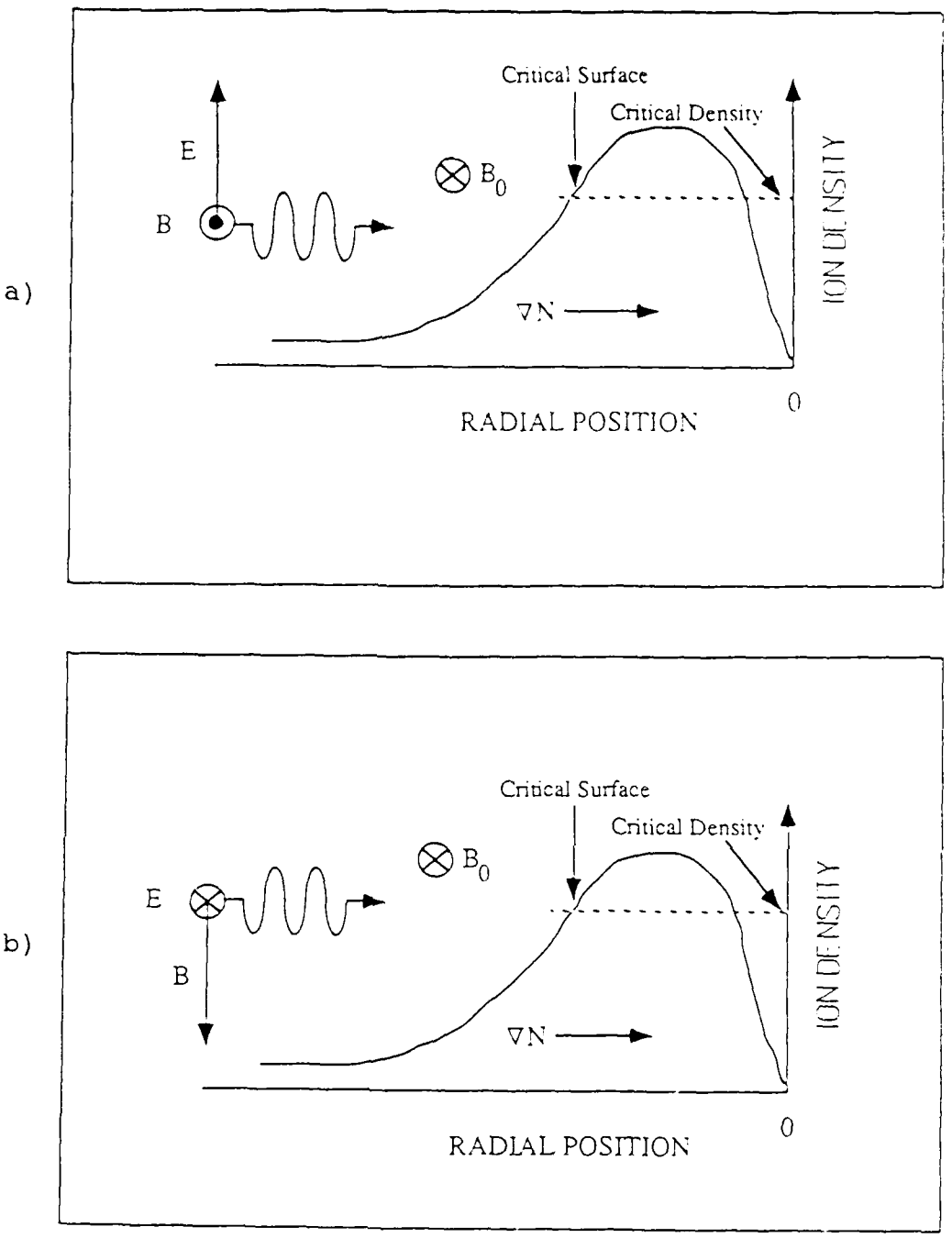


**Figure 2.21.** Sketch showing the geometry of the microwave interaction with the plasma density gradient due to the magnetic confinement. We have idealized to a 2-D geometry. In reality, since $B_0$ is curved, $\nabla N$ is curved, and there is always a component of $E$ along $\nabla N$.

on the plasma, and normally only some component of the electric field exists in this polarization. This simple classification of course assumes a two dimensional geometry. Since the geometry is three-dimensional, a mixture of all three modes is excited. However, predominately one mode will be excited, since the geometry is approximately two- dimensional over the main region of excitation, since the interaction takes place a few magnet radii away from the magnet assembly, and the microwaves have a spatial pattern of approximately the open-ended waveguide.

The present DIMEX experiment is not a good model of microwave interaction with the plasma enclosing a satellite. The reason for this is that in the present DIMEX experiment the microwave wavelength is greater than the relevant plasma scale lengths (diameter and radial density gradient length), while for a satellite the wavelength will be small compared to the relevant plasma scale lengths. However, the instabilities excited should, in general, be similar, and the experiment will provide some understanding of what to expect and help us in designing an experiment to model the real case more accurately.

### 2.4.2 Incident E Parallel $B_0$

For this case, we expect the plasma to behave as if it were a one-dimensional plasma. Otherwise, the magnetic field should have no effect. This polarization is only possible using S-band for the DIMEX experiment, since the L-band waveguide is welded into position and cannot be rotated. Figure 2.22 shows how the relative reflection and transmission vary as the plasma density is increased by increasing the primary electron energy ($\tau$ = 860 $\mu$s). The absorption for ion densities above a density of $10^{10}$ cm$^{-3}$ looks very good. The microwaves reflect off the magnet assembly for no plasma. As the density increases, less and less microwaves get through to reflect from the magnet assembly. This data suggests relative reflectivity on the order of -7.8 dB is possible. (Notes that at 3 GHz the critical density is $1.1 \times 10^{11}$ cm$^{-3}$.)

## 2.5 Incident E Perpendicular to $B_0$ and $\Delta n$

For this case, we expect the microwaves to excite plasma cyclotron waves. This is the orientation of the L-band waveguide, so data at both L- and S-band

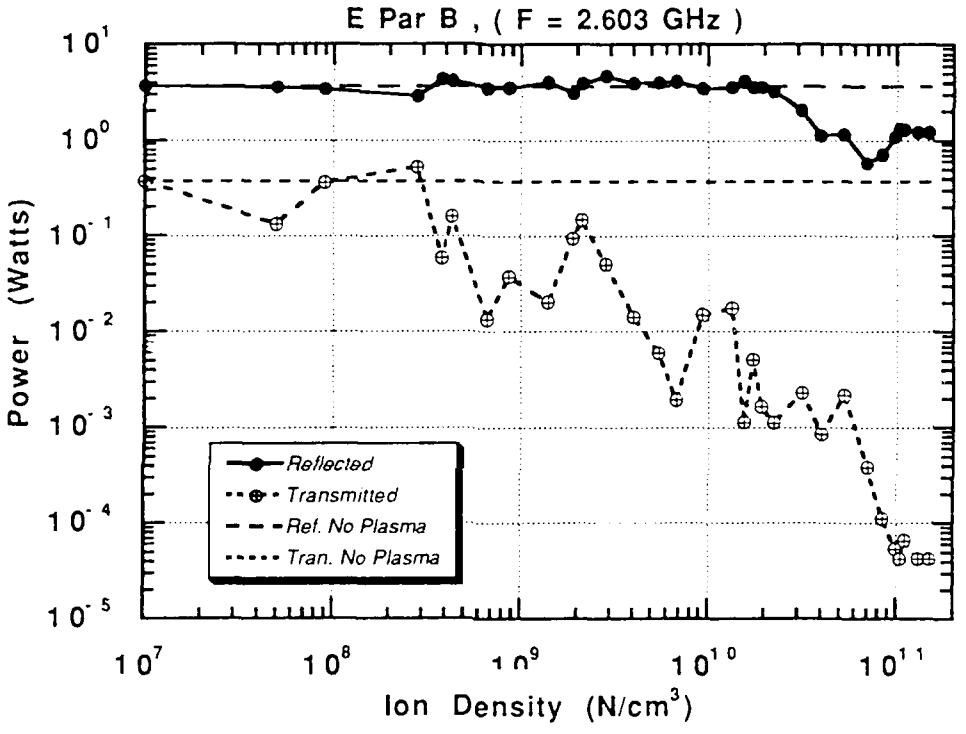


Figure 2.22. Reflected and transmitted microwave power versus plasma density for E parallel to $B_0$ at a frequency of 2.603 GHz.

frequencies are presented in Figure 2.23, although there is only a relatively small density variation. Figure 2.24 covers a larger density variation and shows a strong resonance behavior in the reflected microwaves not seen with the other polarization, as shown in the comparison in Figure 2.25.

The data was obtained by setting the frequency and then increasing the plasma density by raising the primary electron energy. Care was taken to record a few points between every maximum and minimum observed. For normal operation with no chamber walls, no effect would be expected since the density gradient would stretch from the maximum density to zero, and the microwaves would absorb or reflect at the lowest density where the plasma and microwaves were in resonance, e.g. $\sim 1 \times 10^7$ in Figure 2.23. However, in our finite geometry, as the peak density grows, the density at the wall where the microwaves enter also grows. Thus, as the density is increased, we pass through various harmonics of the resonance.

The amount of absorption appears to be frequency-dependent. Thus, at 1.52 GHz, the lowest relative reflectivity appears to be -10 dB, while at 2.6 GHz it is only about -3 dB. A better understanding of this frequency dependence and work to decrease the reflectivity to on the order of -20 dB needs to be accomplished.

Another point to notice is that under some conditions the plasma appears to "duct" the microwaves around the magnet assembly. Thus, in Figure 2.24 for a frequency of 1.251 GHz we see that as the density is increased not only does the reflectivity decrease, but the transmission increases. Since the magnet assembly is in the center of the transmission path between the transmitting and receiving waveguides, the plasma must be bending or ducting the microwaves around the stainless steel magnet assembly. This behavior needs to be better examined.

Finally, for the L-band case we observed that for sufficiently high power (15 watts input power which is about 0.1 W/cm$^2$ for L-band) the absorption process turns off, and the plasma becomes a strong reflector (Figure 2.26). This occurs for power levels much higher than typical radar signals but possibly achievable by high-power microwave weapons. Thus, the DIMEX configuration can turn from a cloak to a shield. We believe this is caused by "profile modification" due to pondermotive force. This process has been observed for laser fusion plasmas and is reasonably well understood for the unmagnetized case and is discussed in more detail in the next

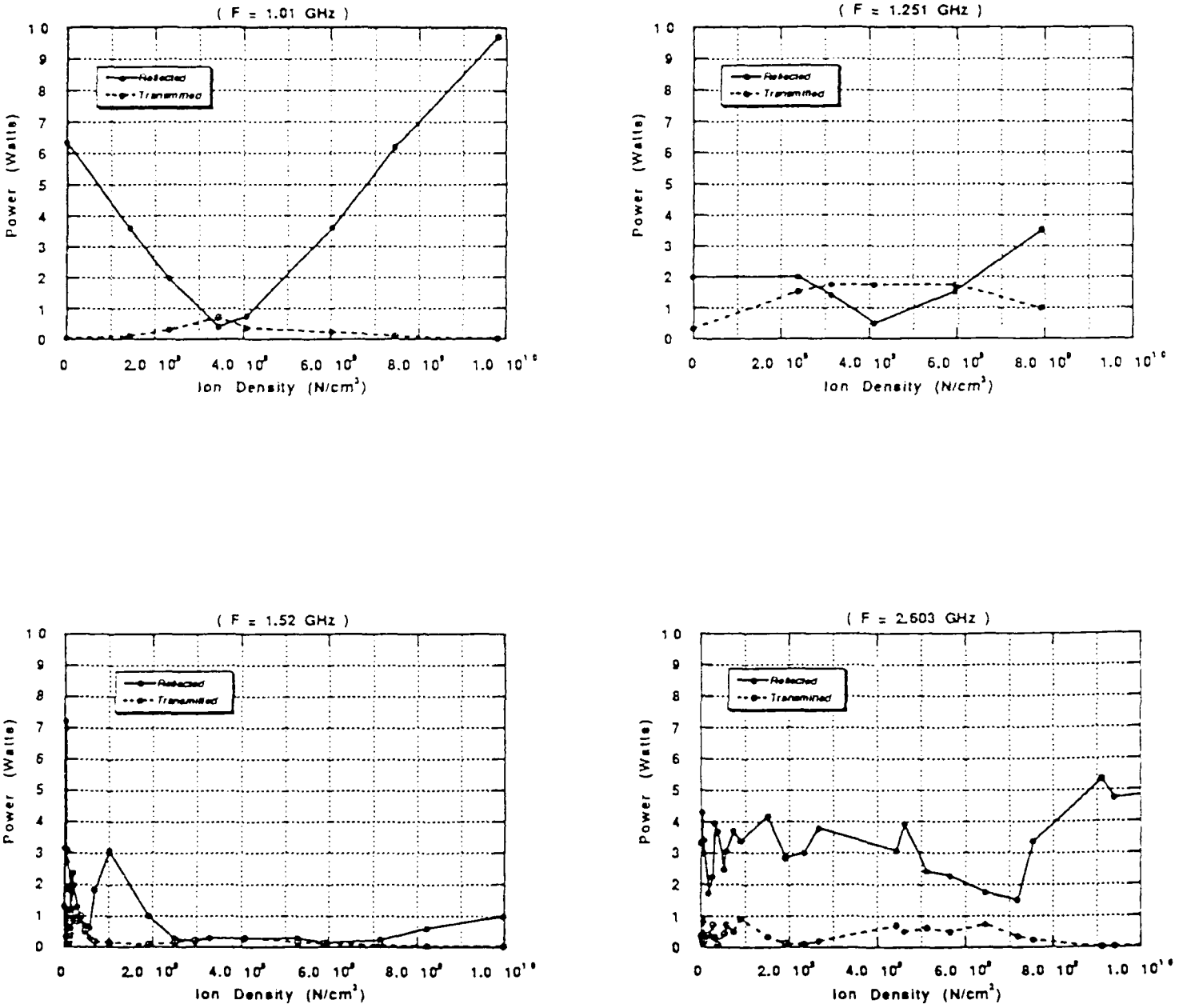


Figure 2.23. Reflected and transmitted microwave power versus plasma density for E perpendicular to $B_0$ and $\Delta n$. Expanded view of plasma density axis and two other frequencies.

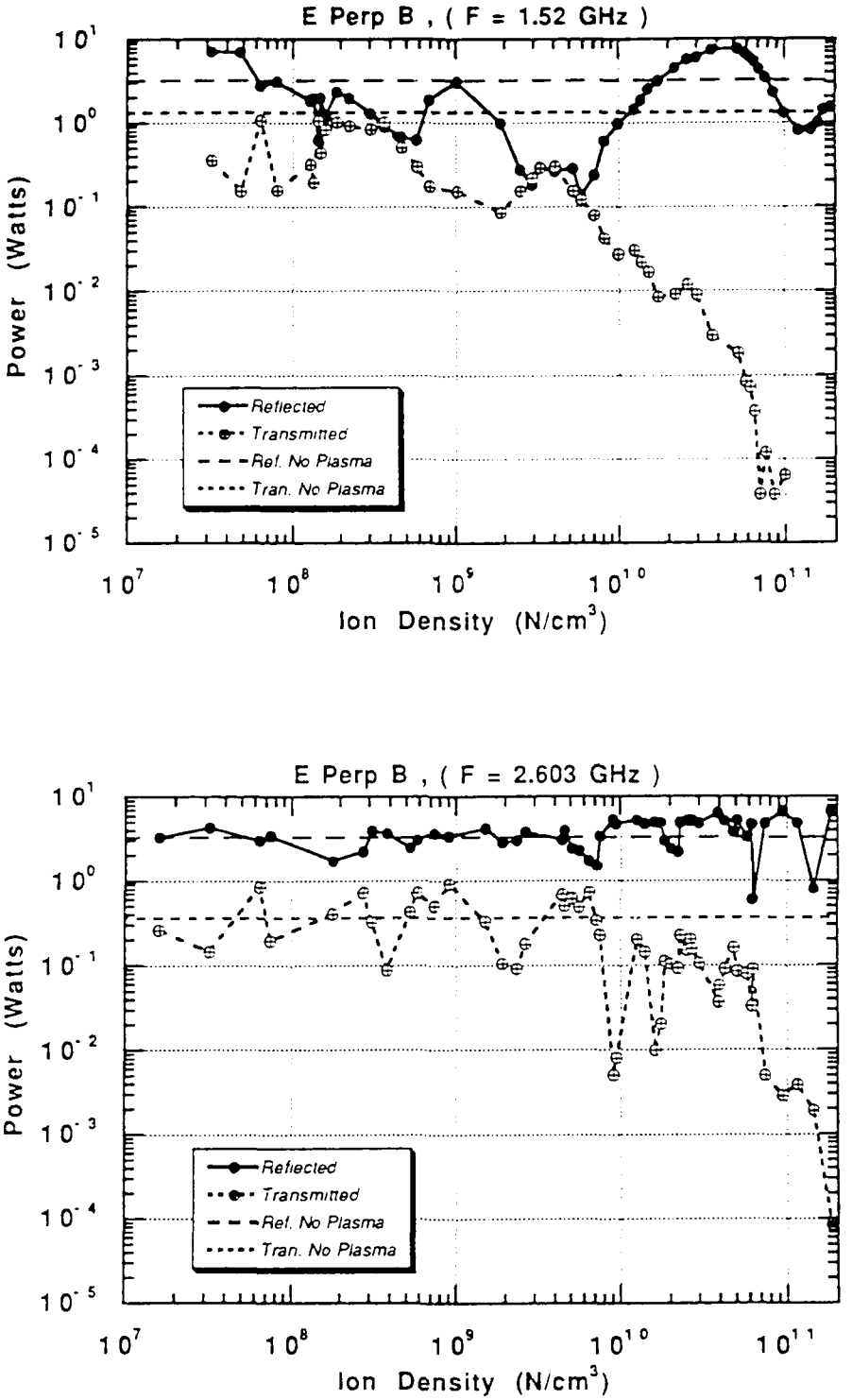


Figure 2.24. Reflected and transmitted microwave power versus plasma density for E perpendicular to $B_0$ and $\Delta n$.

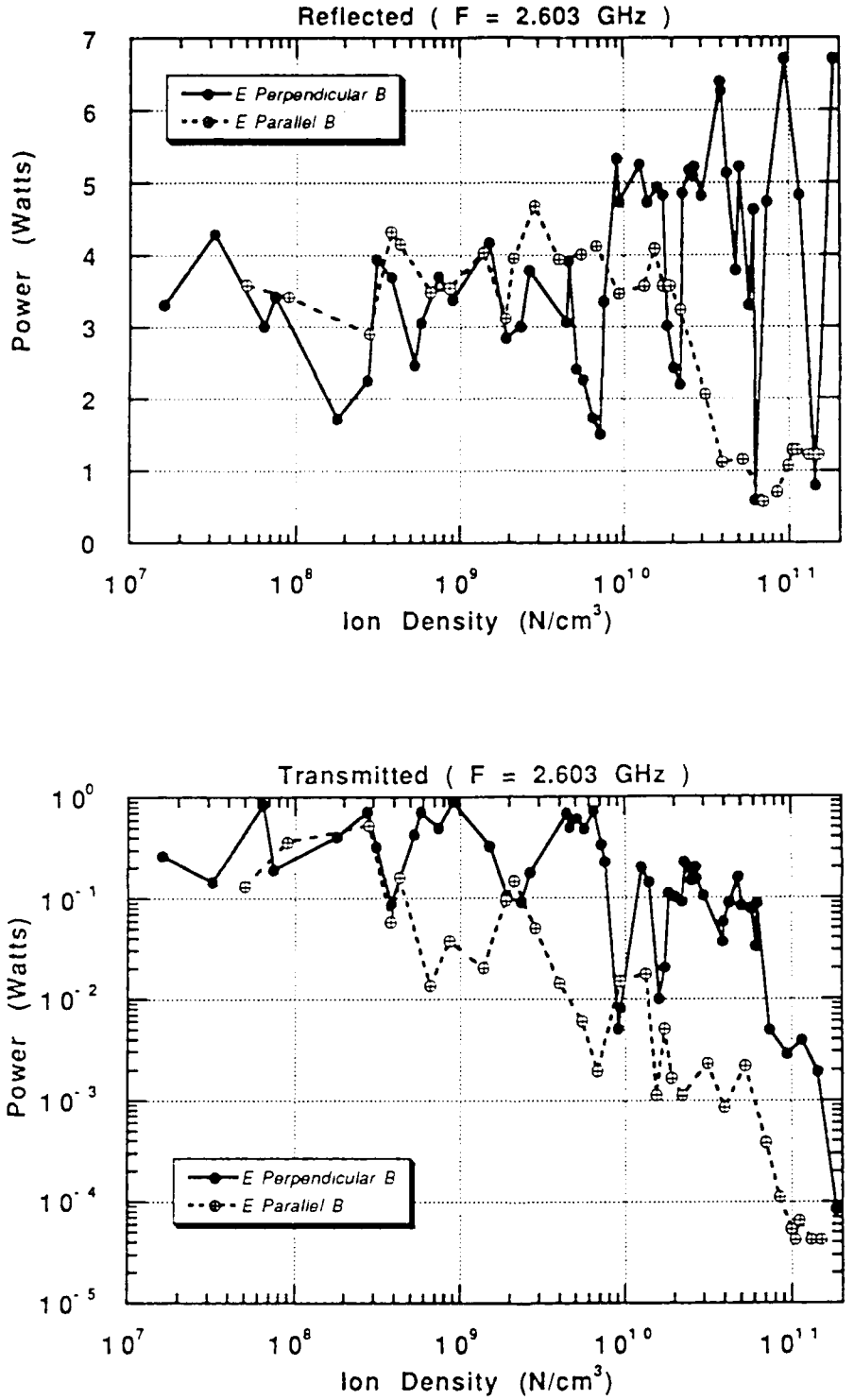


Figure 2.25. Comparison of perpendicular and parallel reflection and transmission.

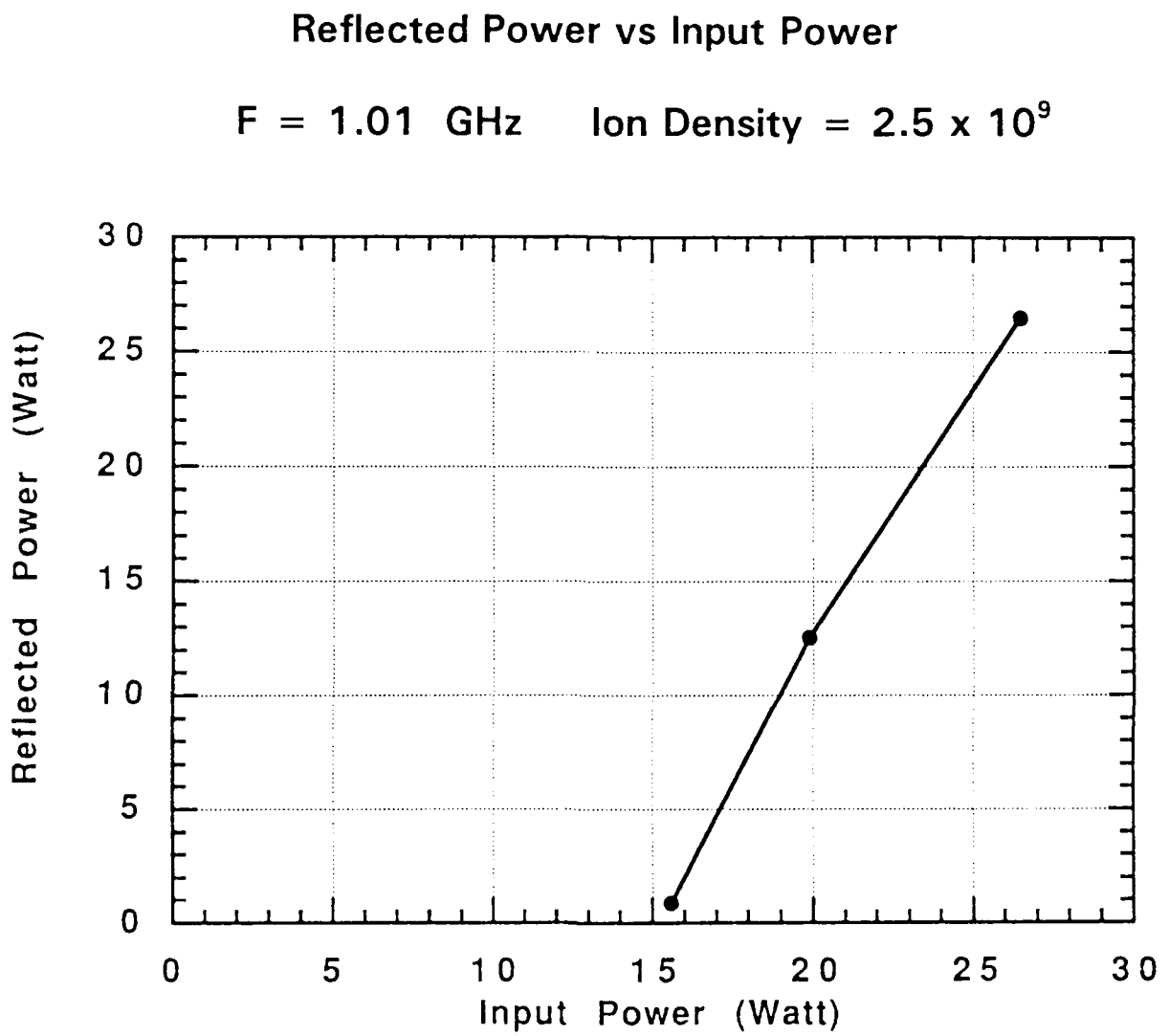


Figure 2.26. Reflected Power vs Input Power for L-band, showing transition from absorption to reflection (cloak to shield).

Section (i.e., 3.4). Further investigation of the shield-to-cloak transition should be carried out in future work.

# SECTION 3

# THEORETICAL ANALYSIS OF DIMEX EXPERIMENTAL RESULTS.

## 3.1 THEORETICAL INTERPRETATION OF DIMEX PLASMA FORMATION AND PROPERTIES.

The formation of the plasma in DIMEX is accomplished by ionizing background argon gas in the experimental chamber with a low voltage ($\sim$ 300 V) electron beam. The beam is launched from a $LaB_6$ cathode at the end of the experimental chamber shown in Figure 3.1. Simulation of the electron beam trajectories over a large range of energies confirmed that electrons would tend to funnel down to strike the pole of the magnet by following magnetic flux lines. These results can be seen in a simulation using the fully EM PIC (Particle-In-Cell) code MAGIC [5]. Results of this simulation can be seen in Figure 3.2.

It was first suggested that this method of creating a plasma on the inner magnetic flux surfaces would not be successful since primary electrons, the electrons from the gun, are excluded from inner flux surfaces. It was reasoned that for plasma to be trapped on inner flux surfaces, as desired, it would have to be formed on those flux surfaces by ionization. However, it appears that the dense plasma is formed in the path of the electron beam on the outer flux surfaces, and that it diffuses rapidly inward via strong turbulence. The plasma is then trapped on the inner flux surfaces when the turbulence ends. This turbulent formation of the plasma is reflected in Langmuir probe traces recording plasma density in time (Figure 3.3) which show that the plasma density rises sharply during the electron beam firing and then relaxes rapidly to a lower value that remains constant for $\sim$ 1 msec before decaying slowly due to diffusion processes.

The properties of the plasma in its densest regions can be summarized as follows: average electron density $10^{11}$ cm$^{-3}$, electron temperature $T_e \sim 1$ eV (11,000 K), ion temperature $T_i \sim 10^{-2}$ eV (room temperature), neutral density $10^{13}$ cm$^{-3}$ (pressure $\sim 10^{-2}$ torr), average magnetic field in dense plasma region $B = 100$ $G$, mean free path for electron neutral collisions, 3 meters, frequency of electron neutral

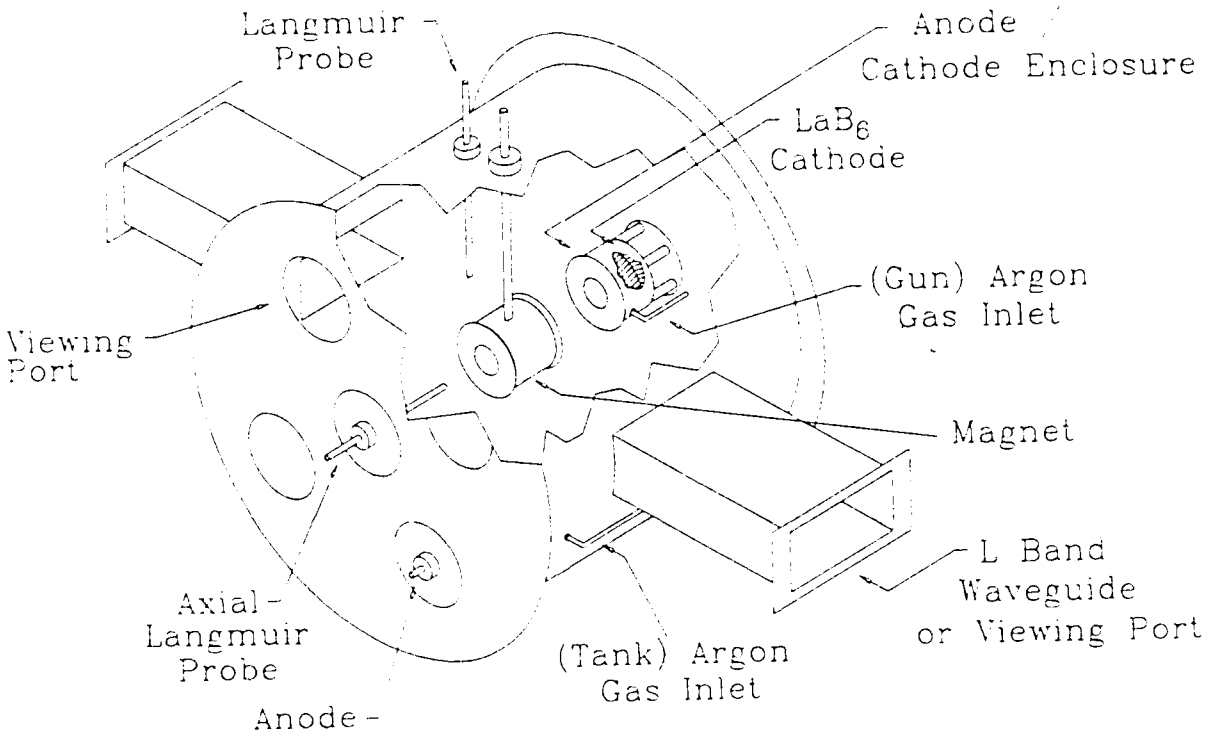


**Figure 3.1. DIMEX apparatus diagram. The DIMEX magnet is located on the axis of the vacuum chamber.**

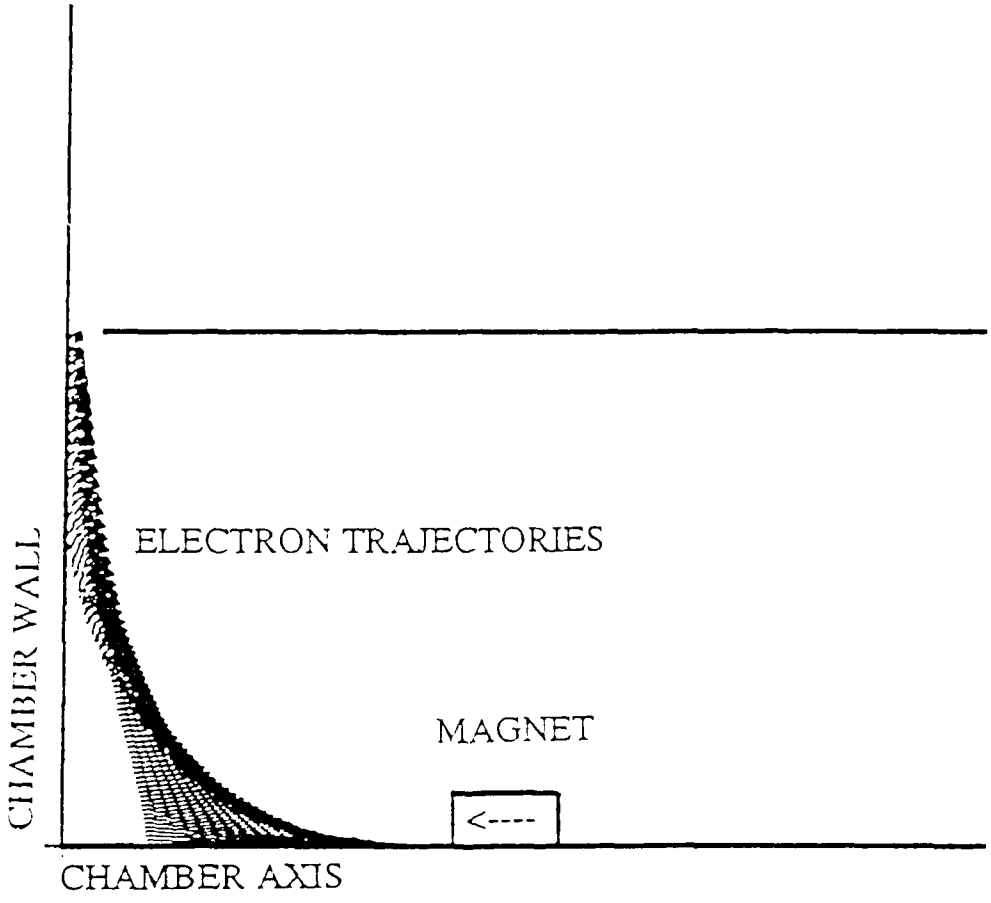


Figure 3.2. MAGIC simulation of electron trajectories in DIMEX. Knowledge of primary electron trajectories in DIMEX can be used to optimize plasma creation and confinement.

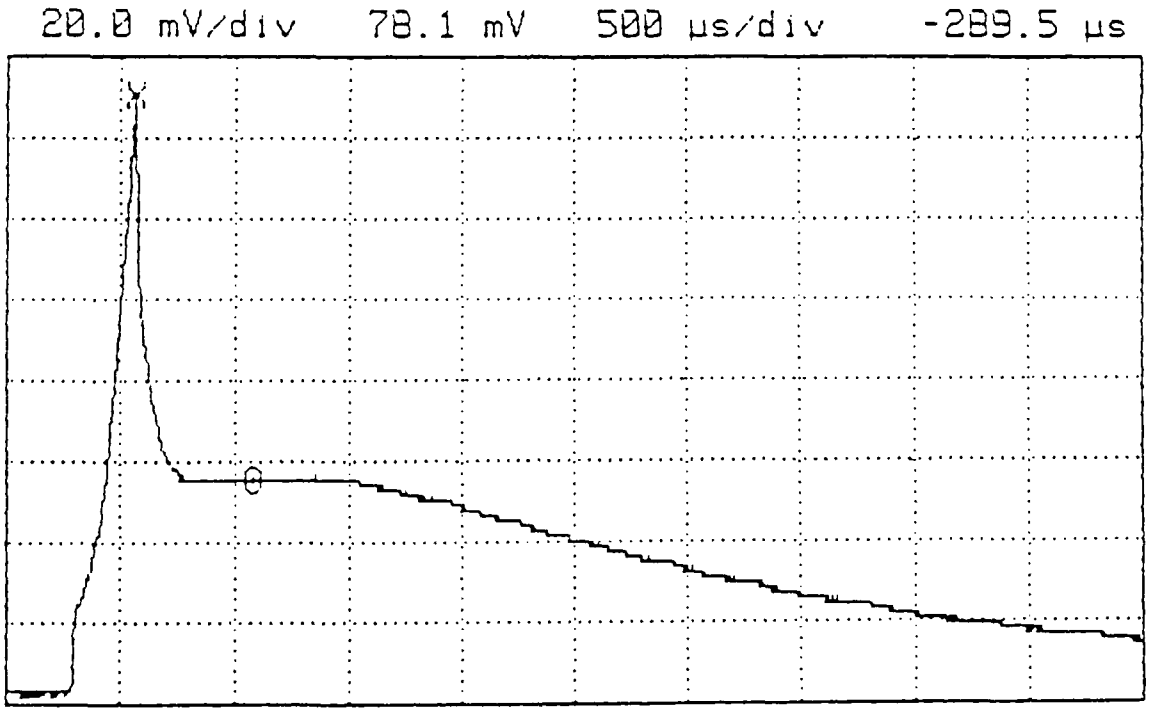


x peak density $1.5 \times 10^{10}$
o plateau density $4 \times 10^{9}$

**Figure 3.3.** **Langmuir probe trace. Plasma density history is consistent with ambipolar diffusion time of 2 msec, indicating possible Bohm diffusion.**

collisions $\nu_{eo} = 2 \times 10^5$/sec, frequency of electron ion collisions $\nu_{ie} = 10^5$/sec, plasma frequency $f_p = 3$ GHz, electron cyclotron frequency $f_{ce} = 2.8 \times 10^8 = .28$ GHz, number of particles in the Debye sphere $N_d = 10^4$, average beta $8\pi nkT_e/B^2 = \beta = 10^{-4}$, Debye length $l_d = 4.2 \times 10^{-3}$ cm, electron gyroradius $r_e = 2.4 \times 10^2$ cm, ion gyroradius $r_i = .6$ cm.

The plasma density appears to vary as $1/r^2$ where r is the radius from the center of the magnet. Because the magnetic field falls off as $1/r^3$ at distances of several radii from the magnet, the plasma will reach $\beta \sim 1$ at roughly 20 cm (ten magnet radii) from the magnet. Because the gyro radii of the electrons and ions are very small relative to the size of the plasma ($\sim$ 10 cm), both electrons and ions can be considered confined.

The plasma is observed to emit a blue light. It is known that the light originates in bound-bound transitions caused by electrons colliding with neutral atoms or ions causing them to go into excited states. Light emission due to atoms excited by electron collision tends to dominate plasma of this density and temperature when neutrals or atomic ions are present, because electron-impact excitation of bound electrons has a much larger cross section than radiative recombination of an electron with an ion or bremsstrahlung, which are the two competing radiative processes. Using $n_e = 10^{11}$, $n_o = 10^{13}$, $T_e = 1$ eV we calculate the radiated power density

$$P = 5.1 \times 10^{-25} K n_e n_o (T_e)^{1/2} \tag{3.1}$$

where $K \sim 1$. This leads to

$$P = 5.1 \times 10^{-1} \text{erg}/(\text{sec cm}^3) \ , \tag{3.2}$$

which gives roughly 1 watt for the entire chamber. Recombination radiation yields

$$P = 1.7 \times 10^{-20} \text{erg}/(\text{sec cm}^3) \ , \tag{3.3}$$

and bremsstahlung is comparable to recombination

$$P = 1.7 \times 10^{-21} \text{erg}/(\text{sec cm}^3) \ . \tag{3.4}$$

Therefore light emission from the plasma is probably due to electron collisions with background neutral atoms and direct impacts of electrons on atomic ions. This suggests that high percentages of ionization in plasmas made from hydrogen can reduce light output by large factors.

## 3.2 MIRROR CONFINEMENT OF THE PLASMA AND THE SHELL PROFILE.

The plasma in DIMEX is observed to form a shell profile, with the high field region nearest the magnet being almost free of plasma, and the plasma density abruptly rising to a peak value at roughly two magnet radii out and then slowly and monotonically decreasing out to the chamber walls. This density profile is shown in Figure 3.4.

This profile can be explained by the theory of plasma confinement and stability in a dipole magnetic field.

The ions and electrons of the plasma will be subject to magnetic forces as they move. In motions transverse to the magnetic field, they will orbit the field lines; however, they will be somewhat free to move in directions parallel to the magnetic field. Parallel to the field lines, the orbiting particles will feel a force repelling them from the strongest part of the field.

$$F = \tilde{m} \cdot \nabla B \tag{3.5}$$

where $\tilde{m} = -m_p v_t^2/(2|B|)$ is the magnetic moment of the particles orbiting the field lines, $m_p$ is the mass of the particle, and $v_t$ is the velocity of the particle transverse to the field line. The magnetic moment of the particle is always opposite the local field direction and has a constant magnitude.

$$m = 1/2 m_p v_{to}^2/B_o \ , \tag{3.6}$$

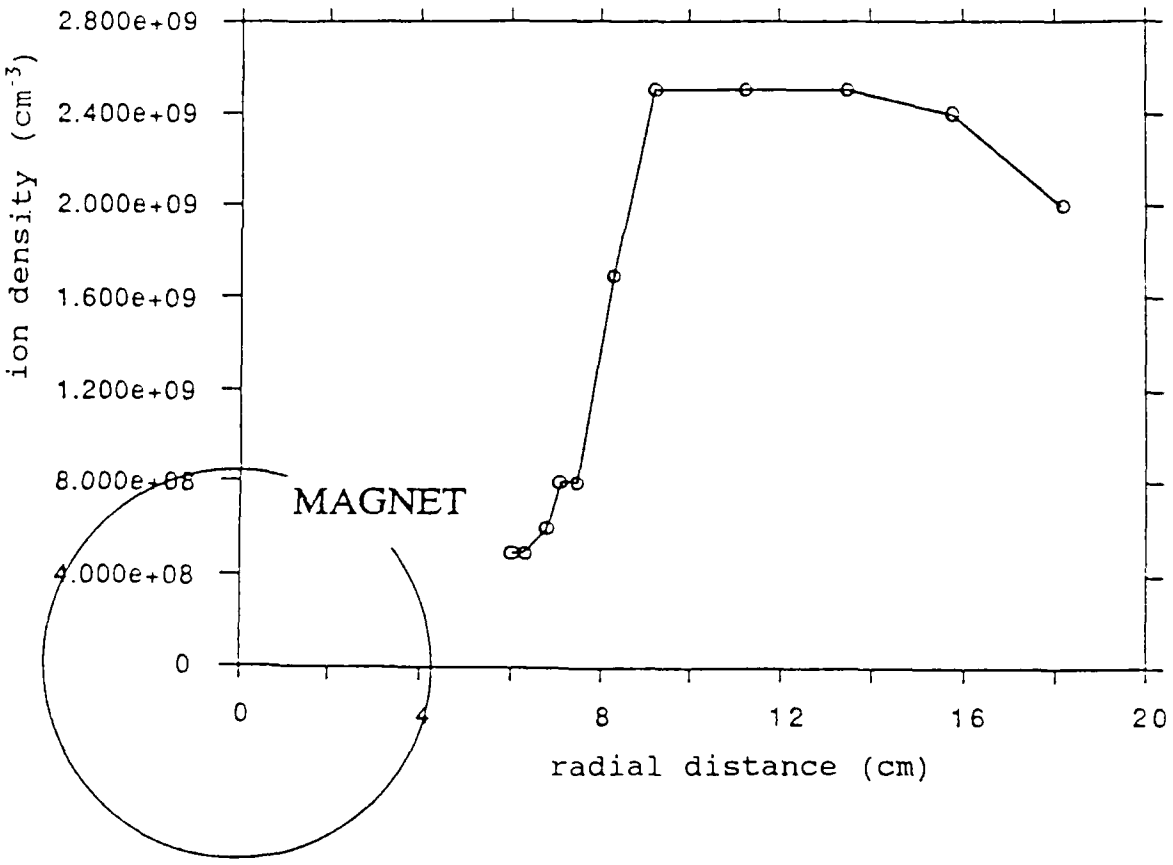


Figure 3.4. Measured plasma density profiles in DIMEX. Plasma appears to be confined on a range of flux surfaces intermediate between the magnet and the vacuum chamber walls.

where $v_{to}$ is the velocity transverse to the field line and $B_o$ is the magnetic field strength where the particle was originally created or diffused on to the field line. We can then write

$$m_p \partial_t v_l = -\bar{m} B \nabla B / |B| \, . \tag{3.7}$$

We can use a vector identity, $\nabla(B^2/2) = B \cdot \nabla B + B \times \nabla \times B$, and the fact that $\nabla \times B = 0$ for a low beta plasma, such as in DIMEX, to obtain

$$m_p \partial_t v_l = -\frac{m_p}{2} v_t^2 |\nabla |B| / |B| \, . \tag{3.8}$$

We then obtain

$$\partial_t v_l^2/2 = (v_t^2/2|B|) v_l \cdot \nabla |B| \, , \tag{3.9}$$

and finally we obtain upon integration

$$(v_l/v_t)^2 = (B_{max} - B_o)/B_o \, . \tag{3.10}$$

From Equation 3.10 it can be seen that ions that have enough energy in the parallel direction will be able to overcome the repulsive force at the poles of the magnet and collide with the magnet surface. If this collision occurs, the ion will immediately recombine with an electron on the magnet surface and cease to be ionized. This ion will be lost to the plasma. A formula for finding the loss criterion of an ion on a field line is as follows:

$$v_l/v_t > (R-1)^{1/2} \, , \tag{3.11}$$

where $R = B_{pole}/B_o$ is the "mirror ratio" on the field line on which the ion is trapped. If $R = 1$, all particles with a velocity vector within a $45^o$ angle of the field line will be lost. This angle defines what is called a "loss cone" of the field line. If $R = 10$, this

angle narrows to 18° so that most of the plasma will be confined. The value of $R$ on a field line for a magnetic dipole is given by

$$R = (b/a)^3 \,, \tag{3.12}$$

where $b$ is the radius of a field line at the magnet midplane and $a$ is the magnet radius, assuming it is a square right circular cylinder. Therefore for $R > 10$, $b/a > 2.15$. The magnet in the experiment is not a perfect dipole, however, so the mirror ratio may be smaller than this. Magnet field measurements, taken on the magnet axis, indicate that at distances of 7 to 10 cm, the magnetic field is well described as a dipole field,

$$B = -\bar{m}/r^3 + 3(\bar{m} \cdot r)r/r^5 \,, \tag{3.13}$$

where the magnetic moment $\bar{m} = 1.53 \times 10^4$ gauss cc. However the magnetic field is weaker at the poles by a factor of $\sim 3$ than the formula indicates. Using the observed radius at the magnet midplane (where the plasma density rises abruptly, and thus indicates the plasma is well confined) gives roughly a loss cone of 30° rather than 20°, and an effective mirror ratio of 3.3 rather than 10.

In any case, all plasma within a radius corresponding to a critical loss cone width will not see a large enough mirror ratio to avoid collision with the magnet poles. If the loss cone is above some critical size, instabilities will occur, because the plasma velocity space will be grossly non-Maxwellian and will cause rapid velocity space diffusion into the loss cone. Effectively, this means that a critical loss cone size and thus critical mirror ratio exists such that all field lines that have a mirror ratio below this value will quickly empty of plasma. The plasma being lost to the magnet surface means a space near to the magnet will clear of plasma within a few microseconds.

Plasma tends to avoid diffusing across field lines into regions of higher magnetic field in the absence of strong turbulence, and for much the same reason, plasma avoidance of higher magnetic fields, the sharp interface between flux surfaces containing substantial plasma and those smaller radii surfaces that contain almost none will be stable to MHD (Magneto Hydro-Dynamic) instabilities. For this reason the

plasma free region in the high-field, low-mirror-ratio region near the magnet will remain plasma free.

The region just outside the plasma-free region near the magnet will contain the peak plasma density. The plasma density will decrease slowly and montonically outward from this point. This monotonically decreasing profile is consistent with the MHD stability of the "interchange" instability produced by "line tying" stabilization of the magnetic flux tubes at the poles. The interchange instability is encountered when magnetic field lines containing plasma have "bad curvature," that is they bow outward, allowing expansion of plasma via interchanges of flux tubes from inner regions to outer regions. This instability occurs when magnetic flux tubes from inner flux surfaces that are full of plasma try to interchange positions with outer flux tubes containing little or no plasma, but an equal amount of magnetic flux. Because of the outward bowing geometry of the flux tubes, the inner flux tubes will expand when they interchange with the outer flux tubes and the outer flux tubes will compress in volume when they interchange. If there were no plasma on the flux tubes or if a uniform plasma were present on all flux tubes, no net change in system energy would occur through an interchange, and the system would be neutrally stable. However, if there is plasma on the inner flux tube, but none on the outer tube, and the two tubes interchange, the plasma on the interchanged flux tube can then expand freely and relieve pressure with no change in magnetic energy. System energy can thus decrease through interchange and plasma can be moved outward in the magnetic field by successive interchanges until it escapes.

This instability is stabilized by the presence of conducting pole pieces that prevent the flux tubes from changing position at the poles by tying them in position. Once tied the flux tubes must flex, increasing their magnetic energy near the poles, in order to interchange. Since the magnetic field is much stronger near the poles and a flexation there will cause a larger magnetic energy change than a flexation in a weaker field region, tying the magnetic field lines near the poles is a high-leverage stabilization mechanism. Line tying thus creates a coupling between thermodynamic energy changes and opposing magnetic energy changes, so that one cannot occur without the other. Accordingly, in a confined plasma with line tying, a balance of pressure and magnetic energy gradients occurs, leading to a stability criterion. This stability criterion can be written, assuming an isothermal equation of state for the plasma, since most of its energy is in the electrons,

$$-rdrP/dr < 4P + 1.33B_o^2\ 8\pi\ . \tag{3.14}$$

This stability criterion requires the normalized pressure decrease with distance always to be smaller than the weighted sum of the local magnetic and thermodynamic pressures. In the DIMEX dense plasma region, magnetic pressure dominates ($\beta = 10^{-4}$) so that stability is satisfied by even a steep decrease. However, the stability criterion can be considered to place a constraint on the steepness of pressure decrease. The observed profile of density and hence pressure (assuming uniform 1 eV temperature) obeys the approximate formula

$$P \sim 1/r^2 \tag{3.15}$$

at long distances. Since $B^2 \sim 1/r^6$ at long distances, the observed pressure profile indicates that we will have $\beta \sim 1$ at approximately 10 magnet radii or 20 cm from the magnet center. Substitution of this profile into Equation 3.14 shows that this profile will be stable, though the formula is derived by assuming $\beta \ll 1$ and thus is not strictly valid for $\beta \sim 1$ regions.

Therefore, the observed shell profile, shown in Figure 3.4, can be explained by lack of sufficient mirror ratio for confinement on inner flux surfaces and the requirement for a slow, monotonically decreasing pressure profile at large radii to satisfy MHD stability. It is probable that more rapid diffusion processes operating at larger radii, where magnetic fields are weaker, will also contribute to the monotonically decreasing profile. The shell profile should be seen to scale geometrically for all magnets of similar geometry, that is, for right circular cylindrical magnets of aspect ratio 1, as in DIMEX, the plasma shell should probably begin at two magnet radii out.

Given that MHD stability limits indicate $\beta \sim 1$ plasmas should be possible, it is likely that much higher plasma densities can be obtained with different plasma formation techniques. The present observed density limits are most likely due to the problems of the outside electron formation technique.

## 3.3 DIMEX PLASMA DENSITY LIMITS AND DIFFUSION.

The plasma density pulse is observed to rise sharply and then drop to a plateau value for approximately one millisecond, from which it begins to decay with a decay time of approximately 2 milliseconds. The density history is shown in Figure 3.3. The plasma density is apparently not limited by MHD instabilities, since it should be stable up to high beta, and its beta is low. Therefore, it appears that the plasma formation process itself imposes limits on the amount of plasma trapped on open field lines.

In a model suggested by Khanh Nguyen of MRC, a virtual cathode forms along the electron beam particle path which lies on the outer flux surfaces. The dense plasma formed in the virtual cathode diffuses rapidly into the magnetic field, because of its turbulence, and becomes trapped on the magnetic flux surfaces once the electron-beam-driven turbulence ends. The electron beam path has been simulated using the fully EM PIC (Particle-In-Cell) code MAGIC and is shown in Figure 3.2. The simulation compares favorably with open shutter photographs where intense light, caused by electron excitation of neutral gas atoms, shows the electron beam path. This dense, *electron-beam-driven plasma* is turbulent and diffuses rapidly into the magnetic field. The plasma density in the system thus rises rapidly near the poles, then relaxes along the flux surfaces once the electron beam which drives the turbulence ends. The plasma appears to remain stable for several milliseconds before instabilities start driving diffusion.

It should be noted that the process outlined here for producing a trapped plasma, though it produces plasmas sufficiently dense for our microwave experiments, is not the method we would use for a Satellite shield. The trapping of the plasma by a turbulent diffusion process means that the plasma becomes trapped in the field only by a random process and thus much more plasma is lost than is retained. Turbulence generally hurts confinement of plasmas in magnetic fields rather than helping it, so that much more plasma is probably lost to the walls than is trapped. An improved process for forming trapped plasmas in the magnetic field is to create a population of mirror trapped ionizing electrons in the magnetic field. This process may allow plasma densities up to MHD beta limits even in the region around the magnet, meaning densities of the order of $10^{14}$.

The decay of the plasma density with time appears to be driven by a diffusion process, rather than by recombination. This can be known with certainty because recombination times are very long in the DIMEX plasma, 16 seconds for radiative recombination and $10^4$ seconds for three-body recombination. Accordingly, the process that limits plasma lifetime appears to be recombination on the solid surfaces in the chamber, which occurs very rapidly once an ion reaches the surface. The ions reach the solid surfaces by diffusion out of the magnetic field. This process chiefly leads to outward diffusion, diffusing out of the strong areas of the magnetic field to the chamber walls rather than inward to the magnet surface.

The diffusion mechanism appears to be a process that takes time to begin, since a millisecond transpires before the plasma begins to decay. The diffusion constant can be estimated from the observed parameters by using Fick's and Gauss' Laws,

$$4\pi/3 < n > \frac{R^3}{T} = 4\pi R^2 D < n > /R \, , \tag{3.16}$$

where $T$ is the observed decay time, $< n >$ is the mean density, $R$ is a mean plasma size, and $D$ is a diffusion coefficient. Using $R \sim 10$ cm as a mean plasma size, we obtain an approximate value for the diffusion coefficient,

$$D = \frac{R^2}{3T} = 1.0 \times 10^5 \text{ cm}^2/\text{sec} \, . \tag{3.17}$$

This is consistent with a Bohm diffusion coefficient for the plasma

$$D_b = cT_e/eB = 6.3 \times 10^4 \text{ cm}^2/\text{sec} \, . \tag{3.18}$$

This diffusion coefficient is much larger than that for ambipolar diffusion driven by collisional processes in the plasma,

$$D_c = \nu_{eo} r_e^2 = 10^{-2} \text{ cm}^2/\text{sec} \, . \tag{3.19}$$

It seems possible, because of the quiescent period seen in the density trace, that instabilities are not occurring for a period and then turning on. This suggests

that instabilities may be inhibited by some mechanism and plasma lifetime increased. It is possible the diffusion is triggered by the perturbing effect of the chamber walls, which empties the outermost flux surfaces of plasma and creates sharp gradients that destabilize the entire density profile. If this is the case, the quiescent period may be extended by simply forming the plasma in a larger vacuum chamber. Ultimately, if this were true, a plasma in space would be extremely long-lived. The issue of loss of plasma from magnetically-confined plasmas is fairly well understood from magnetic fusion theory. We do not believe we are observing any effects that cannot be modeled and inhibited or reduced using presently available theory.

## 3.4 MICROWAVE ABSORPTION AND REFLECTANCE OF THE DIMEX PLASMA.

As part of the DIMEX experiments, microwaves were radiated onto the plasma and reflected signals were monitored as well as signals inside the plasma. As was discussed in the experimental section, absorption was seen at low intensities ($P < 0.1\ W/\mathrm{cm}^2$), but at high intensities, strong reflection was seen. Both of these effects can be explained by coupling of the EM waves to electron plasma waves. Plasma waves and EM waves each cause characteristic motion of electrons. EM waves cause electron motion transverse to the direction of propagation, but plasma waves cause motion in the longitudinal direction (along the direction of propagation). Coupling between the EM waves and the electron plasma waves occurs because of the coupling between transverse and longitudinal motion. Two mechanisms are available for such coupling. One is EM wave induced motion up and down density gradients in the plasma that involves coupling terms of the form,

$$C_1 = v_o \cdot \nabla n_e \ , \tag{3.20}$$

where $v_o = eE/m\omega$ is the electron oscillation velocity in the EM field of amplitude $E$ and frequency $\omega$. The second is EM wave motion coupled to motion up and down density gradients via the action of the B field in the plasma. This has a coupling term of the form

$$C_2 = v_o \times B_o \cdot \nabla n_e / \omega c \ . \tag{3.21}$$

This gives absorption due to electron cyclotron waves. The ratio of growth rates of plasma waves due to these processes is roughly

$$C_1/C_2 = \omega_{ce}/\omega \ , \tag{3.22}$$

which is very small in most regions of high-density plasma, especially at the point where $\omega = \omega_p$, the critical surface of the plasma. At this point $B \sim 10$ gauss and $n_e = 3 \times 10^{10}$, so $\omega_{ce}/2\pi = 2.8 \times 10^{-2}$ GHz and thus $\omega_{ce}/\omega = .028$. Therefore, it is believed that the process of linear conversion of EM waves to electron plasma waves is independent of the polarization of the EM waves relative to the B field direction for high-density plasmas. However, polarization has been seen to affect the reflectivity of the plasma, indicating cyclotron waves may be important.

If we neglect any magnetic-field-produced coupling terms, the pertinent equation for the electron density is

$$\partial_t^2 n_e + \omega_p^2(r) n_e + 3V_e^2 \nabla^2 n_e = \omega v_o \cdot \nabla n_e - \Gamma \partial_t n_e + \omega_{pe}^2 \nabla (v_1 v_o) \ , \tag{3.23}$$

where $\Gamma$ is the damping rate of plasma waves due to collisions or Landau damping, $\omega_p(r)$ is the plasma frequency as a function of $r$, and $v_1$ is the electron motion due to the reflected EM wave. We have for the reflected EM wave,

$$(\partial_t^2 - c^2 \nabla^2) v_1 + \omega_p^2(r) v_1 = v_o \omega_p^2 \frac{n_e}{n_o} \ . \tag{3.24}$$

As can be seen from Equations 3.23, and 3.24, the density fluctuations in the electrons are driven by two terms. One is the nonlinear term due to the pondermotive force and is the product of $v_o$ and $v_1 \sim E_1 E_2$, the electric fields of the incident and scattered waves. The second is a linear term due to electron motion up and down density gradients, that is, the compression and expansion of electron fluid as it moves in response to the EM wave.

The equation for the electron density fluctuations can be considered a driven harmonic oscillator with linear and nonlinear terms as drivers. Obviously, a driver

that generates electron waves at resonance will cause very rapid growth of the waves. The driver will also give up energy to the plasma waves at a high rate at resonance.

According to the equation for $v_1$ (the electron motion due to the reflected EM wave), $v_1$ grows proportionally to the product $v_o\, n_e/n_o$; thus, the nonlinear driving term for the electron waves will be small for small $v_o$ and can be neglected. At low intensities, and thus low $v_o$, the driving term for $n_e$ will be the linear term $\omega v_o \cdot \nabla n_e$. However, if damping rate $\Gamma$ is large, i. e.,

$$\Gamma > \omega v_o \cdot \nabla n_e/n_e \,, \tag{3.25}$$

$n_e$ will not grow at all, in which case the reflected wave will be very small. If $v_o$ is large, however, as in a high-intensity EM wave, it will overcome damping and $n_e$ of the plasma waves will grow rapidly, so that $v_1$ will also grow, and the nonlinear term in Equation 3.24 will become important, and coincidently a reflected wave will grow. Therefore, there are strong theoretical reasons to believe that linear coupling at the critical surface to electron waves will soak up energy and give little reflected power for low-intensity EM waves; however, at high intensities strong plasma waves will grow, consistent with the experimental observations.

At high intensities the nonlinear terms in Equation 3.23 for the electron motion begin to dominate over the linear terms, and plasma waves grow and cause reflection. If the growing waves are electron waves at high frequency, then Raman scattering occurs. However, this instability has a high threshold of power; a similar instability, having a much lower threshold of power, is the SBS (Stimulated Brillouin Scattering) instability.

The SBS instability is a fundamental instability that causes reflection of EM waves from plasmas, even at plasma densities far below critical densities. In the SBS instability, the EM wave scatters off an ion acoustic wave at low frequency in the plasma as opposed to Raman scattering, which involves high-frequency electron plasma waves. The SBS instability comes about fundamentally because plasmas and EM fields interact though Lenz's Law and thus repel each other, EM waves exerting pressure on plasmas and plasmas reacting to shield their densest portions from EM fields. The SBS instability can be summarized by the following sequence of events. An EM wave encounters an ion acoustic wave in a subcritical density plasma; the ion

acoustic wave, because it happens to form a series of regions of differing refractive index at half the EM wave wavelength, acts as a reflecting grating and reflects a portion of the EM wave. The reflected wave forms a standing EM field with the initial EM wave; this standing EM field creates a ponderomotive force that pushes electrons out of the high field regions. The ions follow the electrons; this increases the amplitude of the original ion acoustic wave, which reflects more EM energy and begins the cycle again. Thus, the fundamental hostility between high-intensity EM fields and plasmas manifests itself as the reflection or scattering of high-intensity EM waves off of ion acoustic waves. Since ion acoustic waves are lower frequency and are quasineutral, that is, involve only small charge separations even at large amplitude, these waves are more easily formed by nonlinear processes and thus will have a lower intensity threshold. In addition, SBS does not require a resonance, so it can occur in the subcritical plasma outside the critical surface.

The equations for the SBS instability are as follows:

$$\partial_t^2 n_e - C_s^2 \nabla^2 n_e = R_m n_o \nabla^2 (v_o v_1) \tag{3.26}$$

$$\partial_t^2 \mathrm{hi} - C_s^2 \nabla^2 n_i = R_m n_o \nabla^2 (v_o v_1) \ , \tag{3.27}$$

where $C_s$ is the ion acoustic sound speed $(kTe/m_e R_m)^{1/2}$, where $R_m$ is the ion electron mass ratio, and where the nonlinear terms are proportional to the standing EM field pressure.

A study of SBS instabilities in DIMEX-like plasmas has already been done and found that magnetic field effects consisted only of frequency shifts and had no effect on growth rates. It was also found that these effects were proportional to $(\omega_{ce}/\omega_p)^2$, and these effects are small in DIMEX.

In an inhomogeneous plasma the effect of density gradients acts to introduce a damping effect so the SBS instability will not occur unless the EM wave intensity is high enough. This intensity threshold is given by the expression

$$2/3(v_o/v_e)^2 \omega L/c > 1 \tag{3.28}$$

where L is the density gradient scale length in the plasma. This can also be written as a condition on EM field pressure

$$E^2/8\pi > n_e T_e(\omega/\omega_p)^2/4L \tag{3.29}$$

and can be also written as an intensity threshold

$$P > 3\omega T_e/(r_c L) \tag{3.30}$$

where $r_c = 3 \times 10^{-13}$ cm is the electron classical radius. This becomes, for the DIMEX plasma with L = 10 cm,

$$P > 40 \text{ W/cm}^2 . \tag{3.31}$$

This intensity is larger than the observed threshold for reflection to begin in DIMEX. The difference is probably related to the fact that the microwave wavelength is long, c/f = 30 cm, compared to the plasma size, L $\sim$ 10 cm, for classical SBS to occur.

An alternate approach to calculating the threshold is to use pressure balance since in profile modification the EM field pressure steepens the plasma density gradient near the critical surface. The threshold for this to occur is at an EM wave pressure equal to the plasma pressure at the critical surface, which can be obtained from Equation 3.29,

$$E^2/8\pi \sim n_e T_e \tag{3.32}$$

and which yields

$$P > 50 \text{ W/cm}^2, \tag{3.33}$$

which is close to 3.31. This is again much larger than the observed threshold suggesting that some form of self-focusing of the microwaves by the plasma may be occurring. This would result in higher power densities at the critical surface than 0.1 $W/cm^2$ obtained by taking the incident power and dividing by the waveguide cross sectional area.

The SBS instability does not require a critical density plasma to be effective. High intensity EM radiation can be reflected at high efficiency even at high frequencies, as long as the wavelength is much larger than the Debye length of the plasma, and the EM field pressure does not exceed the plasma thermal energy density. These features were discussed in a previous report.

# SECTION 4

# SUMMARY

The DIMEX experiment has successfully met the original Phase I program goals:

1) Demonstrated confinement of a plasma with high density ($> 10^{11}$ cm$^{-3}$) for long periods of time ($\tau \sim 1$ ms), and
2) Observed strong interaction and absorption of microwaves by the confined plasma (reflection $\sim -10$ dB).

In addition, new insight into how a satellite plasma cloak might work has been obtained:

- Absorption of microwaves occurs at plasma densities several orders of magnitude less than the critical density.
- The confined plasma has low reflectivity due not to just absorption, but also due to "ducting." The plasma appears to diffract the incident microwaves around the "cloaked" object. This is extremely interesting since signals would thus appear to go through the cloaked object making it appear invisible, not just "black."
- For power levels above $\sim 0.1$ W/cm$^2$, nonlinearities set in which result in the plasma becoming highly reflective. Thus, the "cloak" changes to a "shield" when hit by a directed-energy HPM pulse.

Several questions remain unanswered and need to be addressed in a follow-on effort. Foremost is the question of why, even without the magnetic field, long confinement times were observed. We believe this is due to electrostatic confinement, but theory and experiments need to be performed to confirm this speculation. Second, something must be done to confirm that the interactions scale. One approach is to use theory to obtain the scaling behavior. Although such a theory is needed, an experiment with a better scale ratio of microwave wavelength to magnet diameter also should be performed. Such an experiment requires either a larger experimental

chamber or a higher microwave frequency. Since a strong interaction occurs even at relatively low plasma densities, compared to the critical density the latter case is most cost effective. Finally, an understanding of how the plasma "ducts" the microwaves around itself needs to be obtained. Better experimental measurements and theory are required.

## References


1. D. B. Pearlstein, *Journal of Geophysical Research*,Vol. 72, 409, 1967.

2. D. P. Stern and N. F. Ness, *Ann. Rev. Astron. Astrophys.*, **20**, pp. 139-161.

3. J. G. Lafromboise, "Theory of Spherical and Cylindrical Langmuir Probes in Collisionless, Maxwellian Plasma at Rest," Ph. D. Thesis, Institute for Aerospace Studies, University of Toronto, 1966.

4. P. M. Chung, et al. Electric Probes in Stationary and Flowing Plasmas: Theory and Application, Springer-Verlag, New York, 1975, pp. 111-112.

5. B. Goplen, R. Clark, J. McDonald, G. Warren, and R. Worl, "MAGIC User's Manual," Mission Research Corporation Report, MRC/WDC-R-126, April 1987.